

1 EcoTWIN 1.0: A Fully Distributed Tracer-Aided Ecohydrological Model Tracking Water, 2 Isotopes, and Nutrients

3 Songjun Wu¹, Doerthe Tetzlaff^{1,2}, Yi Zheng³, Chris Soulsby⁴

4 1 Department of Ecohydrology and Biogeochemistry, Leibniz Institute of Freshwater Ecology and
5 Inland Fisheries, Berlin, Germany

6 2 Geography Institute and IRI THESys, Humboldt University of Berlin, Berlin, Germany

7 3 School of Environmental Science and Engineering, Southern University of Science and Technology,
8 Shenzhen, China

9 4 Northern Rivers Institute, School of Geosciences, University of Aberdeen, UK

10 Corresponding author: Songjun Wu (songjun.wu@igb-berlin.de)

11

12 Abstract

13 The value of stable water isotopes in constraining process representation in hydrological models is
14 well acknowledged with numerous tracer-aided hydrological models developed in recent years, yet
15 few have leveraged these benefits for more robust water quality modelling. Therefore, we introduce
16 EcoTWIN, a fully distributed tracer-aided ecohydrological model that simultaneously *tracks water*,
17 *isotope*, and *nutrient* fluxes. A thorough model test was conducted by calibrating EcoTWIN against
18 discharge, in-stream isotopes, and NO₃-N concentrations (1980-2024) in 17 large-scale (10³ - 10⁵ km²)
19 European catchments spanning a wide range of geographic and climatic gradients. Furthermore, three
20 reanalysis products (ERA5 snow depth, MODIS evapotranspiration, and GRACE surface water anomaly)
21 were employed to further validate the capacity of EcoTWIN to reproduce associated but uncalibrated
22 internal water fluxes. Results showed good model performance of both calibrated in-stream targets
23 and uncalibrated internal fluxes in most catchments. Therefore, we conclude that EcoTWIN is a flexible,
24 transferable modelling tool for prediction and process inference in terrestrial ecosystems ranging from
25 boreal to subtropic climates. Constrained by tracer simulations, the model not only captures the
26 celerity, but also the velocity of hydrological fluxes, thus providing spatio-temporally-explicit
27 estimations of water ages and travel times. Such information provides opportunities to bridge
28 catchment hydrology and water quality by linking travel times with biogeochemical processing kinetics.
29 We demonstrate this with a proof of concept using Damköhler Number in nitrogen modelling.

30

31 1 Introduction

32 The development of ecohydrological models has been accelerating in the recent decades towards
33 frameworks that are more spatially distributed (instead of lumped or semi-distributed) and complex
34 (integrating more ecohydrological processes) (Pechlivanidis et al., 2011; Wellen et al., 2015). A few
35 examples include SWAT (Arnold et al., 2012), HYPE (Lindström et al., 2010), and mHM-Nitrate (Yang
36 et al., 2018), which have been widely applied worldwide. As process-based models, they are used not
37 only as prediction tools for specific variables, but also as learning tools for model inference, i.e., to

38 track the internal states/fluxes from available observations (Wang et al., 2024). This, however, poses
39 challenges due to the considerable uncertainties in model inference.

40 Inference of internal processes is naturally uncertain due to the lack of direct observations, though
41 such uncertainty can be constrained to some extent by rigorous split-sample calibration and validation.
42 The reason we use “somehow to some extent” here is based on the fact that most models are
43 calibrated to a minimal number of variables, and 81% of calibrations used data from a single gauge
44 (mostly at a catchment outlet) as reviewed in Wellen et al., (2015). Additionally, from a technical
45 perspective, “equifinality” further adds to the inference uncertainty due to the potential
46 misinformation in data (uncertainty in model forcing and observations) and model structure (the use
47 of simplified, abstract mathematics to simulate real world processes) (Beven, 2006). This can result in
48 inaccurate process representations yielding deceptively good results through error compensation,
49 thus leading to overconfidence in a model's ability to reproduce within-basin dynamics (Wen et al.,
50 2024; Wu et al., 2025a). As acknowledged by the hydrological community, models calibrated solely
51 against discharge at the catchment outlet reflect only the celerity of hydrological systems (pressure
52 wave propagation), yet constituent transport in water quality modelling relies on the velocity (mass
53 flux of the water) (McDonnell & Beven, 2014). Failure to reconcile these differences can lead to
54 questionable process inferences from many ecohydrological and water quality models.

55 One way to strengthen model inference is to include auxiliary data for calibration (Efstratiadis &
56 Koutsoyiannis, 2010). However, there is a paradox in multi-criteria calibration, as on the one hand,
57 more auxiliary data will feed unique information to the calibration process, thus effectively
58 constraining the model behaviour from an ecohydrological perspective; yet on the other hand, it
59 increases the dimensionality of calibration thus resulting in degraded performance or failure of
60 calibration from a technical perspective. The “curse” of dimensionality in ecohydrological modelling is
61 universal for all the commonly used algorithms under both Bayesian and Pareto theories as
62 demonstrated in Wu et al., (2025c). Therefore, modellers should expect the selected auxiliary data to
63 contain as much information as possible (Nearing et al., 2020). For distributed modelling, the auxiliary
64 data should reflect the cumulative contribution of all upstream reaches/regions, rather than variables
65 that are highly dependent on local condition/processes (e.g. point-scale soil moisture and
66 evapotranspiration measurements etc.).

67 Stable water isotopes, in this context, have powerful potential in cumulative flux tracking. As
68 conservative tracers, ^2H and ^{18}O are independent of biogeochemical reactions and naturally integrate
69 landscape heterogeneity, thus providing effective constraints on spatially distributed (dis)connections
70 of hydrological flow paths as well as velocity of the hydrological systems which reflect flux-storage
71 interactions (Jung et al., 2025; Tetzlaff et al., 2015). The value of tracers has long been recognised by
72 hydrologists (Hooper et al., 1988), with many tracer-aided hydrological models developed and evolved
73 in recent years from lumped (Birkel et al., 2011; Godsey et al., 2010), to semi-distributed (van
74 Huijgevoort et al., 2016; Nan et al., 2021), and distributed structure (Kuppel et al., 2018; Remondi et
75 al., 2018). However, few attempts have been made to integrate a tracer-aided hydrological structure
76 into water quality modelling (Birkel & Soulsby, 2015; Jung et al., 2025), despite the need being evident

77 for nearly four decades (Neal et al., 1988). Moreover, existing pioneering models are mostly
78 conceptualised/lumped (Benettin et al., 2015; Dick et al., 2015) and/or loosely coupled via external
79 tracer/water quality modules (Pesántez et al., 2023; Yang et al., 2024; Zhang et al., 2020). The external
80 coupling of model chains transfer necessary internal states and fluxes between sub-models (e.g.
81 hydrological fluxes for constituent mixing in water quality or isotopic modules) via online in-memory
82 coupling (instead of offline on-disk coupling), thus significantly increasing the resources consumption
83 in input/output operations. Such model chains, though providing useful scientific insights, can become
84 problematic for large-scale applications owing to the exponential growth in computational and
85 storage requirements. Therefore, there remains a need to develop a fully distributed, computationally
86 efficient ecohydrological model that combines hydrological, isotopic, and water quality simulations.

87 This research gap motivated the development of EcoTWIN, the model that we present in this paper.
88 To our knowledge, the model is one of the first distributed tracer-aided **ecohydrological** models that
89 **tracks water, isotopic, and nutrient** fluxes simultaneously in a C++-based framework. For a thorough
90 testing of EcoTWIN, 17 large European catchments were selected for calibration against discharge, in-
91 stream isotopes, and NO₃-N concentrations. These catchments span over a wide range of geographic
92 (Alpine to lowland plain) and climatic (from snow-dominated to Mediterranean) gradients. In addition,
93 the robustness of modelled inference on uncalibrated internal fluxes were also compared with three
94 remote sensing products (snow depth, evapotranspiration, and water storage). Given the overall good
95 integrated performance in most catchments, EcoTWIN is presented as an ecohydrological modelling
96 framework applicable for terrestrial ecosystems ranging from boreal to temperate and subtropical
97 climates across a wide range of geographical environments. The subsequent sections are organised as
98 follows: Section 2 and 3 introduce the model structure of EcoTWIN and details in calibration and
99 validation; the model performance is shown in Section 4; in Section 5 we show the advantages of a
100 tracer-aided ecohydrological framework with an example of how water ages bridge catchment
101 hydrology and water quality models; finally, the current limitations and planned future development
102 of EcoTWIN are also discussed.

103

104 **2 Model description**

105 EcoTWIN is fully distributed ecohydrological model implemented in C++. The model consists of
106 hydrological, isotopic, and nitrogen modules, which simulate major ecohydrological states and fluxes
107 from canopy to groundwater (Figure 1). Aided by tracer simulations, the model is additionally able to
108 track the water movement vertically and laterally via the calculation of water ages and travel times.
109 For detailed information of model parameters please refer to Table S1.

110

111 **2.1 Hydrological module**

112 EcoTWIN follows a typical multi-layer, top-down, bucket-type approach that resolves the water
113 balance sequentially for the vegetation canopy, three soil layers, unsaturated zone, and groundwater.

114 As the foundation of solute transport, the hydrological module employs a selective disassembly
 115 structure with multiple alternative conceptualisations possible for specific important hydrological
 116 processes. The configuration can be specified *a priori* based on the goal of modelling and prior
 117 knowledge of the studied catchment(s).

118 **2.1.1 Soil properties**

119 Before iterative simulations, soil characteristics are estimated using appropriate pedotransfer
 120 functions. Three different alternatives are provided, each of which requires different levels of inputs
 121 but all were found to provide robust estimation of soil porosity (θ_s), field capacity (θ_{fc}), wilting point
 122 (θ_{wp}), and hydraulic conductivity (Ks). All the soil properties are required for each soil layer/depth.
 123 This can be achieved via three alternative options: (i) assigning identical properties across the whole
 124 soil column, (ii) calculating separately for each depth based on depth-dependent inputs, or (iii)
 125 extrapolating deeper profile characteristics from the top soil properties based on a depth-dependent
 126 equation in Maneta & Silverman, (2013).

127 The distribution of soil types and land use is assigned from raster file in EcoTWIN. This can be specified
 128 as a static boundary condition; alternatively, the distributions can also be updated dynamically via a
 129 user-specified interval to reflect any temporal changes due to land management.

130

131 **2.1.2 Vertical fluxes**

132 The vertical fluxes are resolved for storages in the canopy, soil layers, unsaturated zone, and
 133 groundwater. The mass balance of canopy storage (ΔC) follows:

$$\Delta C = P - I - Th \quad (1)$$

134 where P , I , Th are precipitation, interception, and throughfall, respectively. The throughfall is
 135 calculated as the exceedance of current canopy storage from the maximum storage calculated by Leaf
 136 Area index LAI and a correlation parameter α .

$$C_{max} = \alpha * LAI \quad (2-1)$$

137 Alternatively, the maximum canopy storage can be estimated with explicit consideration of
 138 precipitation intensity (Landgraf et al., 2023):

$$C_{max} = \alpha * LAI * \left(1 - \frac{1}{1 + SCF * P / (\alpha * LAI)}\right) \quad (2-2)$$

139 where SCF is the vegetation cover fraction calculated by LAI and an extinction coefficient (rE)
 140 adopted from HYDRUS-1D (Šimůnek et al., 2013):

$$SCF = 1 - \exp(-rE * LAI) \quad (3)$$

141 Then throughfall is calculated as the exceedance of canopy storage from the maximum:

$$Th = (P + C) - C_{max} \text{ if } (P + C) > C_{max} \text{ else } 0 \quad (4)$$

142 After reaching land surface, throughfall becomes ponding water (S_{Pond}) or snow (S_{Snow}) depending
 143 on a temperature threshold for separation ($Thre_{SN}$). Snow will melt and recharge the ponding water
 144 in warm conditions (air temperature Ta exceed $Thre_{sn}$) following a degree-day model.

$$melt = S_{snow} * \min(dd_{min} + dd_{inc} * Th * (Ta - Thre_{SN}), dd_{max}) \quad (5)$$

145 Where dd_{min} and dd_{max} are the minimum and maximum of degree day factor, while dd_{inc} denotes
 146 the rate of increase in the degree-day factor per degree Celsius rise in temperature.

147 The available ponding water infiltrates into the top soil layer using Green-Ampt model (Kale & Sahoo,
 148 2011; Maneta & Silverman, 2013), with infiltration capacity first calculated as a function of average
 149 soil moisture over the hydrologically active depth:

$$I_f = K_s * \left(1 + \frac{\psi * \theta_s * (1 - (\theta_1 - \theta_{wt}) / (\theta_s - \theta_{wt}))}{\theta_1 * d_1}\right) \quad (6)$$

150 Where θ_1 , θ_s , θ_{wt} , and d_1 are the moisture content, porosity, wilting point, and depth in top soil layer;
 151 ψ is a parameter representing soil air entry pressure in m. Then potential infiltration (F_p) is determined
 152 from the lesser between the available ponding water (S_{pd}) and potential infiltration rate integrated
 153 over time before ponding occurs ($I_f * t_p$).

154 The actual infiltration (F) is solved iteratively using the Newton–Raphson scheme:

$$F = \Delta\theta * d_1 = F_p + K_s * w_{Ks} * (\Delta t - t_p) - \psi \Delta\theta * \ln\left(\frac{\psi \Delta\theta + \Delta\theta d_1}{\psi \Delta\theta + F_p}\right) \quad (7)$$

155 where w_{Ks} is anisotropy ratio of vertical to horizontal K_s .

156 The soil storage in each layer is conceptualised as two water pools – a gravitational, free-flowing pool
 157 and a capillary, soil-bound pool. The two pools are separated based on field capacity (Maneta &
 158 Silverman, 2013), and percolation happens when soil storage exceeds the threshold. Three alternative
 159 schemes are included in EcoTWIN.

160 In the first scheme, all water in excess of field capacity percolates to deeper layer:

$$Pc_i = (\theta_i - \theta_{fc}) * d_i \quad (8-1)$$

161 where Pc_i , θ_i and d_i depict the percolation, moisture content and depth from/in i th soil layer in m.

162 The second scheme additionally considers the hydraulic conductivity (K_s) following the
 163 conceptualisation in SWAT (Arnold et al., 2012):

$$Pc_i = (\theta_i - \theta_{fc,i}) * d_i * \left(1 - \exp\left(\frac{-\Delta t * K_s}{\theta_{s,i} - \theta_{fc,i}}\right)\right) \quad (8-2)$$

164 The third scheme relates percolation to the extent of soil saturation with an exponential parameter β
 165 (Kumar et al., 2013; Samaniego et al., 2010):

$$Pc_i = (\theta_i - \theta_{fc,i}) * d_i * \left(1 - \exp(\beta * \log(\theta_i / \theta_{s,i}))\right) \quad (8-3)$$

166 For evapotranspiration, soil evaporation and transpiration are estimated separately. The separation
 167 of PET is realised by surface cover fraction introduced above:

$$PT = PET * SCF; \quad PE = PET - PT \quad (9)$$

168 Soil evaporation is simulated in the top soil layer based on the soil saturation:

$$Evap_s = PE * \min\left(\frac{\theta_1}{\theta_{fc,1}}, 1\right) \quad (10)$$

169 Transpiration is simulated in all soil layers based on the fractions ($f_{root,i}$) of root density ($D_{root,i}$) in
 170 each layer partitioned by soil depth and a parameter (γ_{root}):

$$Tr_i = PT * f_{root,i} * \frac{\theta_1 - \theta_{wp,1}}{\theta_{fc,1} - \theta_{wp,1}} \quad (11)$$

$$f_{root,i} = D_{root,i} / \sum_{j=1}^m D_{root,j} \quad (12)$$

$$D_{root,i} = \left(1 - \gamma_{root}^{\left(\sum_{j=1}^m d_j\right)}\right) - \left(1 - \gamma_{root}^{\left(\sum_{j=1}^i d_j\right)}\right) \quad (13)$$

171 Channel evaporation is also estimated using Penman equation, which relies on net radiation, wind
 172 speed, air pressure, and air temperature as inputs.

173 The last soil layer percolates to an unsaturated storage in unsaturated zone (S_{unsat}). The
 174 compartment stores the excess water from soil and percolates either downward to groundwater
 175 storage (S_{GW}) or laterally downstream. The percolation to groundwater P_{CGW} is determined by a
 176 weighting parameter p_{GW} as a proportion of unsaturated storage:

$$P_{CGW} = S_{unsat} * p_{GW} \quad (14)$$

177 Additionally, irrigation is conceptualised in EcoTWIN, which is realised via the water extraction from
 178 river or groundwater. The source is determined by the geographic location: for a grid cell with channel
 179 network, water is extracted directly from river, and local groundwater is used as irrigation source for
 180 non-channel grids. The amount of extraction is estimated from a predefined coefficient for crop water
 181 demands (w_{irr}) from which the deficit is calculated for each of the m soil layers.

$$deficit = \sum_{i=1}^m (\theta_{fc,i} - \theta_{wp,i}) * w_{irr} * d_i \quad (15)$$

182 Note that the irrigation can switch to groundwater extraction if river storage cannot fill the deficit.

183

184 **2.1.3 Lateral fluxes**

185 In EcoTWIN, grid cells are connected laterally at three levels - surface, unsaturated zone, and
 186 groundwater. Note that some models omit the unsaturated storage and directly calculate excess
 187 water to drain based on the saturation extent of the bottom soil layer (e.g., ECH₂O-iso, Kuppel et al.,

188 2018). EcoTWIN did not follow this conceptualisation because in reality, the lateral drainage is focused
 189 in the saturated zone, and thus the bottom of the soil layer instead of the whole soil profile. The
 190 drainage of an entire soil layer thus brings considerable uncertainty to the velocity of lateral transport
 191 when the lower boundary of the soil is a parameter to tune in calibration. For instance, a large soil
 192 depth will dramatically reduce the velocity of interflow drainage and slow down the mixing of
 193 constituents, though this might still perfectly reproduce the celerity (hydrograph) for purely
 194 hydrological modelling. Our conceptualisation (an independent unsaturated compartment) aligns
 195 with most hydrological models (Arnold et al., 2012; Yang et al., 2018) and fits the recent analysis
 196 supporting the dominant role of lateral drainage over vertical transports globally (Mcmillan et al.,
 197 2025).

198 By the end of each timestep, ponding water receives upstream inputs and contributes to channel
 199 storage if the grid is connected to the channel network, while non-channel grid has $Ovf_C = 0$:

$$Ovf_C = (Ovf_{T,in} + S_{pond}) * p_{Ovf} * dx_C/dx_T \quad (16)$$

200 dx_C and dx_T are the channel length and size of terrestrial grid cell; p_{Ovf} is a weighting parameter for
 201 channel recharge. Then the remaining ponding water routes to downslope terrestrial grid following
 202 the topographic gradient. In none-channel grid cells, all available ponding storage routes lateral
 203 downstream ($Ovf_C = 0$):

$$Ovf_{T,out} = (Ovf_{T,in} + S_{pond}) - Ovf_C \quad (17)$$

204 Similarly, unsaturated storage contributes first to channel storage in grid cells within channel network,
 205 while non-channel grid cells have $Inf_C = 0$:

$$Inf_C = (Inf_{T,in} + S_{vadose}) * K_{vadose} * \left(1 - e^{-1 * exp_{Inf} * (Inf_{T,in} + S_{vadose})}\right) * p_{Inf} \quad (18)$$

206 where K_{vadose} is the effective conductivity of lateral transport in the unsaturated zone; while exp_{Inf}
 207 is an exponential parameter determining the strength of positive correlation between recharge and
 208 current unsaturated storage. Then the remaining unsaturated storage is partially routed to downslope
 209 grid cell following a linear approximation of Kinematic wave equation, which assumes gravitational
 210 flux per unit width $Inf_{T,out}$ is proportional to the subsurface hydraulic conductivity (K_{vadose}) and
 211 bedrock slope ($slope$ approximated from the surface slope):

$$Inf_{T,out} = (Inf_{T,in} + S_{unsat} - Inf_C) * \left(1 + \alpha * \frac{dt}{dx}\right) * \alpha * \frac{dt}{dx} \quad (19)$$

$$\text{where } \alpha = K_{unsat} * \sin(slope)$$

212 Groundwater routing is similar to that of interflow, with channel recharge followed by terrestrial
 213 transport. Note that the terrestrial groundwater flow does not consider the bedrock slope as
 214 groundwater storage is generally much large than unsaturated storage, and thus independent from
 215 topographic gradients:

$$GWf_C = (GWf_{T,in} + S_{GW}) * K_{GW} * \left(1 - e^{-1 * exp_{GWf} * (GWf_{T,in} + S_{GW})}\right) * p_{GWf} \quad (20)$$

$$GWf_{T,out} = (GWf_{T,in} + S_{GW} - GWf_C) * \left(1 + \alpha * \frac{dt}{dx}\right) * \alpha * \frac{dt}{dx} \quad (21)$$

where $\alpha = K_{vadose}$

216 The channel routing is realised using Kinematic wave equation based on a scaled channel roughness
217 parameter (Maneta & Silverman, 2013).

218

219 **2.2 Isotopic module**

220 The isotopic module in EcoTWIN tracks the composition of stable water isotopes in all water storage
221 compartments following hydrological mixing and fractionation. The module also provides estimation
222 of water age and travel time conceptualised as the time since water molecules enter the catchment
223 as precipitation, and the time water molecules need to travel through the specific storage.

224 **2.2.1 Mixing**

225 The mixing and transport of isotopes (^2H and ^{18}O , both noted as C) are governed by the velocity of
226 hydrological fluxes with a complete mixing strategy for most water storages:

$$\frac{d(V * C)}{dt} = \sum_{k=1}^{N_{in}} q_{in,k} * C_{in,k} - \sum_{k=1}^{N_{out}} q_{out,k} * C \quad (22)$$

227 Where V and C are the volume and composition/concentration of the storage, while N_{in} and N_{out}
228 denote the number of influx and outflux. Such strategy is built on two assumptions: (i) constitutes (i.e.,
229 isotopes) are fully mixing within each timestep; (ii) the composition/concentration in outflow equals
230 to that in storage. Additional mixing between ponding and upper soil water storage is allowed (with
231 proportion determined by a parameter $SrfMixing$), as nutrients in top soils can be flushed out in
232 large hydrological events (Seybold et al., 2022).

233 The full-mixing assumptions have been widely used and shown to be reasonable for storages with
234 relatively small volumes in many mixing/water quality models (Arnold et al., 2012; Yang et al., 2018).
235 However, some studies show that a complete mixing strategy can be problematic for large storages
236 such as groundwater as they are generally poorly constrained (e.g. Soulsby et al., 2015). Therefore,
237 the mass conservation equation used in the INCA-N model and mHM-Nitrate is employed to calculate
238 the mixing of groundwater storages with influxes (i.e., percolation from unsaturated storage and
239 lateral groundwater inflow).

$$\frac{dC}{dt} = \frac{1}{V + V_r} * \left(\sum_{k=1}^{N_{in}} q_{in,k} * C_{in,k} - \sum_{k=1}^{N_{out}} q_{out,k} * C \right) \quad (23)$$

240 where V_r is the retention storage. The equation is solved by the fourth order Runge-Kutta technique.

241

242 **2.2.2 Fractionation**

243 As conservative tracers, the composition of isotopes in water storages/fluxes is only changed by
 244 kinetic fractionation apart from hydrological mixing. The process is accompanied by evaporation,
 245 resulting in the preferential loss of lighter isotopes (^1H and ^{16}O) to the vapor phase and a
 246 corresponding enrichment of heavier isotopes (^{18}O and ^2H) in the residual water. In EcoTWIN, the
 247 fractionation is simulated along with evaporation of top soil water and river storage based on the
 248 Craig-Gordon model (Craig et al., 1964; Kuppel et al., 2018), while transpiration is assumed to be a
 249 non-fractionating process (Dawson & Ehleringer, 1991; Kuppel et al., 2018).

$$C = C^* - (C^* - C) * \left(\frac{S - Evap}{S} \right)^m \quad (24)$$

250 where C^* and m are the limiting isotopic composition (in ‰) and the dimensionless enrichment slope
 251 that are estimated via the following equations in (Good et al., 2014):

$$C^* = \frac{h_a C_a + h_s \varepsilon^+ + \varepsilon^k}{h_s - h_a + \varepsilon^k / 1000} \quad (25)$$

$$m = \frac{h_a - (h_s \varepsilon^+ + \varepsilon^k) / 1000}{h_s - h_a + \varepsilon^k / 1000} \quad (26)$$

252 where h_a is the relative humidity above the soil surface normalised from atmospheric relative
 253 humidity (h), air temperature (T_a), and soil temperature (T_s estimated from Amato & Giménez, 2024).
 254 C_a is the isotopic composition of ambient air moisture estimated from precipitation composition:

$$C_a = (C_{rain} - \varepsilon^+) / \alpha^+ \quad (27)$$

255 where ε^+ is the equilibrium fractionation factor (Skrzypek et al., 2015); α^+ is a temperature factor
 256 estimated from T_a .

$$\varepsilon^+ = (1 - 1/\alpha^+) * 1000 \quad (28)$$

257 The factor of diffusion-controlled kinetic isotopic separation ε^k is calculated based on the relative
 258 humidity of soil surface (h_a) and soil pore (h_s).

$$\varepsilon^k = (h_s - h_a) * \left(1 - \frac{D_i}{D} \right) * n \quad (29)$$

259 Where D_i and D denote the diffusivities of water vapor molecules containing heavier isotope and the
 260 lighter isotope, respectively. The ratio can be acquired in Horita et al., (2008) for ^2H (0.9877) and ^{18}O
 261 (0.9859). n is an advection term ranging between 0.5 (in saturated soils) and 1 (in dry soils). The factor
 262 is included in calibration for the fractionation of top soil evaporation yet fixed as 0.5 for that of channel
 263 evaporation.

264

265 **2.2.3 Water age and travel time**

266 EcoTWIN can track the age of water i.e., the time since water enters the catchment as precipitation,
267 in each storage. In age tracking, precipitation is defined as new water with age of zero. At the end of
268 each time step, water ages of all storages are advanced based on the temporal resolution (for instance
269 one day if the model is set up for daily timesteps). Note that in some circumstances, the modellers
270 might need to disable the age evolution of specific storage(s) (e.g., groundwater storage) as the
271 storage can be too large to achieve steady states in model spin-up. Similar to isotopes, water ages are
272 only controlled by hydrological transport with the same mixing strategy (i.e., complete mixing except
273 for groundwater).

274 The water ages in EcoTWIN are the mean values averaged from all water molecules in the storage,
275 which might be dominated by the inflow of very old water that obscure the age distribution of the
276 young water (e.g., the groundwater input to top soils due to the groundwater extraction for irrigation).
277 Therefore, EcoTWIN additionally provides the estimation of travel time - the time of water molecule
278 travelling through each storage. The simulation is similar to that of water ages. The only difference is
279 that the transition of water between storages (e.g., percolation into deeper soil layers) resets the travel
280 time to zero. Accordingly, all the water enters a new storage becomes new water instead of just
281 precipitation in water age tracking.

282

283 **2.3 Nitrogen module**

284 The nitrogen module describes the mass balance of nitrogen, particularly nitrate as the main form of
285 dissolved nitrogen, which is dominated by the interaction of hydrological transport and
286 biogeochemical transformations.

287 For each timestep, the nitrate concentration is simulated in each storage following three processes –
288 hydrological transport/mixing, nitrogen inputs, and biogeochemical transformations. Fully integrated
289 with hydrological module, nitrate transport also aligns with hydrological fluxes following the same
290 mixing strategy as in the isotopic simulation. For nitrogen sources, EcoTWIN considers the inputs from
291 fertiliser, manure, and plant residues, whose annual inputs can be specified via configuration. Notably,
292 fertilization can be parameterised via spatial raster inputs if corresponding dataset is available. The
293 timing and extent of nitrogen addition of all sources are determined following the implementation in
294 HYPE (Lindström et al., 2010), which distributes the annual sum across a specified period (e.g., the
295 period between planting and harvest for crops). Additionally, wet deposition is conceptualised as the
296 atmospheric nitrogen source, whose concentration can be specified via spatial raster and simply as a
297 constant value.

298 The biogeochemical transformations are mainly modified from the mHM-Nitrate model (Yang et al.,
299 2018), and the HYPE model (Lindström et al., 2010), which are conceptualised for the soil profile and
300 channel network. In the soil profile, three nitrogen pools are conceptualised for each soil layer,
301 including an inactive nitrogen pool (SN_i), an active nitrogen pool (SN_a), and a dissolved nitrate pool

302 (DN). The soil transformations include degradation (Dgd_s , from SN_i to SN_a), mineralisation ($Minr_s$,
 303 from SN_a to DN), denitrification ($Deni_s$, from DN to gaseous N_2), and plant uptake ($Uptk_s$, DN
 304 removal).

$$Dgd_s = SN_i * ref_{Dgd,s} * f_{Ta} * f_{\theta} / dt \quad (30)$$

$$Minr_s = SN_a * ref_{Minr,s} * f_{Ta} * f_{\theta} / dt \quad (31)$$

$$Deni_s = DN * ref_{Deni,s} * f_{Ta} * f_{\theta,deni} * f_{conc,s} / dt \quad (32)$$

305 where $ref_{Dgd,s}$, $ref_{Minr,s}$, $ref_{Deni,s}$ are the parameters representing the reference rates of soil
 306 degradation, mineralisation, and denitrification. f_{Ta} and f_{θ} are the regulating factors of temperature
 307 and moisture.

$$f_{Ta} = 2^{(T_a - 20)/10} * \omega \quad \text{where } \omega = \begin{cases} 1 & T_a > 5 \\ T_a/5 & 0 \leq T_a \leq 5 \\ 0 & T_a < 0 \end{cases} \quad (33)$$

$$f_{\theta} = \min \left[\frac{(1 - p_{\theta,deni}) * (\theta_{fc,i} - \theta_i)}{p_{\theta,fc} * d_i}, \frac{(\theta_i - \theta_{wp,i})}{p_{\theta,wp} * d_i} \right] \quad (34)$$

308 where $p_{\theta,fc}$ and $p_{\theta,wp}$ are the empirical factors that are fixed as 1.2, 0.8 based on literature values
 309 (Lindström et al., 2010; Yang et al., 2018). $p_{\theta,deni}$ is the saturation threshold for soil denitrification
 310 ranging between 0.4 – 0.85 (Yang et al., 2018). A different moisture factor considering a saturation
 311 threshold (θ_{thres}) is employed for denitrification, as denitrification is more sensitive to the soil
 312 wetness condition:

$$f_{\theta,deni} = [(\theta_i / \theta_{fc,i} - \theta_{thres}) / (1 - \theta_{thres})]^{2.5} \quad (35)$$

313 The process is additionally controlled by the concentration level in the storage $f_{conc,s} = C / (C + 10)$.
 314 Plant uptake is simulated using a three-parameter logistic growth equation in (Eckersten et al., 1994;
 315 Lindström et al., 2010).

316 Currently, in-stream denitrification is the only process considered in EcoTWIN.

$$Deni_w = ref_{Deni,w} * f_{Tw} * f_{conc,w} * A / dt \quad (36)$$

317 where $ref_{Deni,w}$ is the reference in-stream denitrification rates. The actual rates are regulated by a
 318 concentration factor $f_{conc,w} = C / (C + 1.5)$ and a temperature factor f_{Tw} (the same equation for f_{Ta}
 319 with inputs substituted by river temperature f_{Tw} , simplified as the rolling-average of 20-day air
 320 temperature).

321 It should be noted that the calibrated soil depth in this study is about 2.5 m, with intermittent
 322 saturation occurring in the deeper layer. This means that terrestrial denitrification is a combination of
 323 soil and groundwater processes in this study, though this might change in other applications if a
 324 shallow soil depth is assigned.

325

326 **3 Model calibration and validation**

327 A robust model application should not only reproduce observed variables through calibration but also
328 yield realistic estimates of internal states and fluxes that are not included in the calibration process.
329 This is essential to avoid situations where inaccurate process representations produce deceptively
330 good results through error compensation. Therefore, we evaluate EcoTWIN from both perspectives.
331 First, we assess the model's ability to reproduce observations via calibration (methods and results in
332 Sections 3.2 and 3.4). Then, we examine the model's capacity to simulate uncalibrated internal states
333 and fluxes by comparing the simulated snow depth, evapotranspiration, and total water storage with
334 corresponding remote-sensing products (methods and results in Sections 3.3 and 3.5).

335 To ensure model generality, 17 catchments were selected for calibration and validation depending on
336 the data availability (particularly stream stable water isotopes and nitrate), which span a wide range
337 of characteristics in geography, climate, and anthropogenic managements (~~Figure 2 and Table~~
338 ~~1~~catchment locations, characteristics, and major hydrological and nitrogen inputs are shown in
339 Figure 2, Table 1, and Figure S1, respectively). Anthropogenic management practices have a less
340 dramatic effect than climate and geography in most catchments due to the relatively low proportion
341 of urbanized areas. However, a few notable exceptions—such as the Rhine, Elbe, and Danube
342 catchments—are included in the analysis, as these densely populated regions hold critical ecological,
343 agricultural, and economic importance for Europe, and are subject to intensive human interventions
344 in water management. This also provides a chance to examine the applicability of EcoTWIN in human-
345 affected catchments.

346

347 **3.1 Model setup**

348 EcoTWIN was setup for each of the 17 catchments for calibration with a spatial resolution of 5 km²
349 and a temporal resolution of daily timesteps from 1980 to 2024 (with first two years for spin-up). As
350 a fully distributed model, gridded GIS inputs are used in the model setup, including a digital elevation
351 model, flow direction, slope, channel width, channel length, proportion of each land use type (Winkler
352 et al., 2021), proportions of each soil type (world soil map, WRB2014), and soil properties (e.g., depth-
353 dependent proportions of clay, sand, silt, and organic matter from SOILGRIDS). All spatial inputs were
354 acquired with finer resolution (50 m or above) and resampled to the resolution of this application (5
355 km).

356 The climatic variables used to drive EcoTWIN include precipitation, air temperature, potential
357 evapotranspiration, relative humidity, and a few variables that are optional required for the
358 calculation of channel evaporation (air pressure, net radiation, and wind speed). These climatic
359 variables are available from the reanalysis products ERA5 and E-OBS, while PET is calculated using FAO
360 Penman-Monteith equation. For nitrogen simulations, additional inputs are needed including the
361 fertilization map (Grizzetti et al., 2021) and nitrate concentration of rainfall (Zhu et al., 2025) as the
362 boundary of nitrogen addition from agricultural activities and wet deposition.

363

364 3.2 Model calibration

365 **Method.** The calibration was conducted separately for each catchment to test the applicability of
366 EcoTWIN under different geological and climatic contexts. Three commonly used variables for
367 hydrological and water quality modelling (discharge, stream water isotope composition, and in-stream
368 NO₃-N concentrations) are employed for calibration. Their long-term time series were acquired at daily
369 steps from different sources (discharge from GRDC, isotopes from Wateriso and GNIR, and NO₃-N
370 concentration from global water quality database, GEMStat), and then compared with simulation
371 results at multiple sites for each catchment. Here ¹⁸O was selected for isotopic validation due to its
372 higher precision and data abundance. Given the discrepancy in duration of observations (especially
373 for isotopes and NO₃-N), a separate calibration and validation based on a split-sample approach is
374 difficult. Therefore, the full timescale (1982 - 2024) was used for calibration (and the validation
375 introduced in Section 3.3).

376 The Differential Evolution Adaptive Metropolis algorithm (DREAM) was selected for parameter
377 optimisation due to its relatively efficient and effective performance for high-dimensional problems
378 (as benchmarked in Wu et al., 2025c). The algorithm was implemented separately for each catchment
379 with the same prior distribution of parameters (Table S1). The maximum iteration was set as 100,000
380 for each catchment (20 chains with maximum chain length of 5000), from which 40 best simulations
381 were selected from the posterior distribution. The Kling-Gupta efficiency (KGE) statistic was used to
382 construct an informal likelihood function for DREAM optimisation.

$$l = \left[\sum_{i=1}^{N_{obs}} \sum_{j=1}^{N_{site}} (1 - KGE) * w_{i,j} \right]^{-m} \quad (37)$$

383 Where l is the likelihood; N_{obs} and N_{site} are the number of observation types (discharge, isotopes,
384 and nitrate) and sites. The weight $w_{i,j}$, defined for observation type i at site j , is assigned equally
385 across sites such that the total weight for each observation type sums to 1/3. m is an exponentially
386 coefficient to stretch the likelihood surface that is often set based on the number of observation points.
387 After prior test run, m was set as 500. Finally, the likelihood function is transformed to logarithmic
388 form for numeric stability. The calibration was validated using Kling-Gupta efficiency (KGE), Root Mean
389 Square Error (RMSE), Pearson Correlation Coefficient (Coefficient), and Percent bias (Pbias) (Table 2).

390 **Calibration performance.** EcoTWIN successfully reproduced the observed discharge in all 17
391 catchments with KGE exceeding 0.5 at most site (Figure 3a3A&D; Table 2). Such performance is
392 comparable to or better than previous continental calibration of hydrological models (e.g., ParFlow,
393 Naz et al., 2023; E-HYPE, Donnelly et al., 2016).

394 Similarly, isotopic and nitrate simulations also produced acceptable performances at most sites (Figure
395 3b3B; Table 2). However, there are a few exceptions. The failure of isotopic simulations was found at
396 two sites within the AlpineAlps region (bottom-left corner of figure 3b). This can be attributed to the
397 uncertainty in precipitation isotopes and snowmelt isotopes (due to the lack of snowmelt elution

398 ~~fractionationsnow elusion fractionation~~; Ala-aho et al., 2017), the incorrect isotopic composition in
399 groundwater, or the reduced applicability of degree-day model for mountainous areas in Europe. Such
400 simulation deviation due to the uncertainty in data and boundary initialisation is often reported in
401 previous calibration (Smith et al., 2021).

402 ~~In general,~~As for nitrogen simulation (Figure 3C), the model produces comparable performances to
403 existing nitrogen modelling at catchment (Wu et al., 2022, 2025b; Yang et al., 2018) and continental
404 scales (Jones et al., 2023; Mikayilov et al., 2015). ~~However, nitrate~~The degraded nitrogen simulations
405 ~~failed to capture the observations at three sites, though as is shown~~were found coarsely across Europe,
406 ~~but they are mostly~~ in ~~Figure S1, these all have relatively~~rivers/stream with low levels of NO₃-N
407 concentrations ~~given the low RMSE in Table 2~~. Such low average values can easily trigger the
408 degradation in KGE as one of the sub-components of KGE is highly sensitive to the mean deviation,
409 though the absolute deviation remained low ~~(Figure S1 and Table 2)~~. Overall, we concluded that
410 EcoTWIN has good capacity to reproduce in-stream components for a wide range of catchments and
411 for relatively long periods.

412

413 3.3 Model validation

414 **Method.** Remote sensing or reanalysis products were further employed to validate uncalibrated
415 internal model states or fluxes from three important perspectives in ecohydrological modelling – snow
416 depth from ERA5, evapotranspiration from MODIS, and surface water mass anomaly from GRACE (as
417 a storage proxy). The simulated variables corresponding to these products are, respectively, the depth
418 of snow pack, the sum of soil evaporation, channel evaporation, and transpiration from all soil layers,
419 and the anomaly of total water storage above groundwater (i.e., the sum of canopy storage, snow,
420 soil water storages, and unsaturated storage). The validation was realised via resampling the remote
421 sensing products to 5 km and comparing grid-to-grid with the modelled outputs. r^2 was used as the
422 performance metrics, as KGE is not applicable for time series with zero average, yet the average of
423 surface mass anomaly is close to 0.

424 Note that all three products may contain considerable uncertainties. ERA5 is a reanalysis product that
425 combines historical observations into global estimates using modelling and data assimilation
426 approaches, therefore inevitably embeds uncertainties associated with model structure and
427 observational coverage (Hersbach et al., 2020). MODIS evapotranspiration is derived from remotely
428 sensed spectral information, energy partitioning approaches and the Penman–Monteith framework,
429 whose uncertainty may exceed 30% depending on spatial scale and environmental conditions (Mu et
430 al., 2011). GRACE infers changes in terrestrially stored water masses from spatial and temporal
431 variations in the Earth's gravity field; however, its coarse spatial resolution can introduce substantial
432 uncertainty when used for hydrological validation, particularly at basin or sub-basin scales (Tapley et
433 al., 2004). Nevertheless, good agreement between simulations and remote sensing or reanalysis
434 products can enhance confidence in the robustness of simulated spatial and temporal patterns,
435 although it does not necessarily imply accurate representation of absolute magnitudes.

436 **Validation performance.** First, we compared the sum of soil evaporation, channel evaporation, and
437 transpiration to MODIS evapotranspiration in each grid cell. The results in Figure 4S2 and Table 3
438 shows a general good fit between simulation and MODIS records with ~~KGE and r^2~~ coefficient of
439 determination (R^2) above 0.5 in most ~~regions. From the subplots~~ selected catchments. This is further
440 validated after zooming into two representative catchments (W5 Nemunas and W10 Rhine) in Figure
441 4, we can see that 4A-B, where KGE reaches above 0.5 in >80% of the catchment domain. The other
442 evaluation metrics (RMSE, Pearson coefficient, RMSE, and percent bias shown in Table 3) also
443 demonstrated the seasonality and magnitude good performance of evapotranspiration ~~were well~~
444 captured though the peaks in summer were slightly underestimated simulations.

445 Then, the surface water ~~storagemass~~ anomaly from GRACE was compared to the anomaly of simulated
446 surface storage, i.e., the sum of canopy storage, snow, soil water storages, and unsaturated storage.
447 The grid-to-grid comparison in Figure 44C-D shows a general good an acceptable fit in most regions
448 with r^2 close to or R^2 above 0.5-3 in around half regions in catchment Nemunas (W5) and Rhine (W10),
449 as well as other European catchments (Figure S3 and Table 3). However, more degradation in
450 performance was found compared to ~~the performance in~~ evapotranspiration, ~~especially in coastal~~
451 ~~regions.~~ simulation. For instance, the validation in Rhine shows degraded water storage simulation in
452 Alpine regions. This is likely due to the locally complex topography and the simplified representation
453 of snow accumulation and melt processes in the model, which struggle to capture the high spatial
454 variability of storage in mountainous terrain. Besides, we also found degraded performance in coastal
455 regions. For example, GRACE exhibited considerably increasing trends in water storage between 2005
456 to 2015 in two Nordic catchments (W2 and W3; Figure S3), yet our simulations only showed a
457 moderate increasing trend. Similar degraded performance was found in the coastal catchments (e.g.,
458 three British catchments W6-8 in UK; Figure S3), though the magnitudes of simulation and GRACE data
459 fit well. This is possibly attributed to the coarse resolution of GRACE which ~~additional~~ additionally
460 considered the storage mass from ocean in coastal region yet not included in this terrestrial-explicit
461 modelling.

462 Finally, the simulated snow depth was compared to the daily snow depth in ERA5 reanalysis products
463 (ERA5 post-processed daily statistics on single levels; 10.24381/cds.4991cf48). Results in Figure 44E-F
464 show a generally good agreement between simulations and ERA5 records with $R^2 > 0.5$ in most regions
465 with $r^2 > 0.5$, though in Nemunas and Rhine. Though degradation was found in a few other catchments.
466 Note that, the poor performances were generally found in (e.g., W14-17 in Figure S4), these
467 catchments with generally experienced limited snow accumulation, e.g., W14-17 in subplots in Figure
468 4. In the other words, the absolute deviation was relatively limited for snow depth simulation.
469 demonstrated by low RMSE in Table 3

470

471 **4 Water age simulation and its link to water quality**

472 Like many existing distributed hydrological and water quality models (e.g., SWAT, mHM, Ech₂O-iso,
473 HYPE etc.), EcoTWIN can provide estimation of the main ecohydrological fluxes at high spatial and

474 temporal resolutions, including canopy interception, snow melt-accumulation, infiltration, percolation
475 through soil layers, groundwater recharge, and lateral flux routing at different horizontal phrases.
476 Among these variables, a unique trait of EcoTWIN lies in its capacity to track water fluxes via isotopes,
477 thus being able to provide a consistent estimate of water age and travel times. Therefore, in Figure 5,
478 ~~both these~~ variables are shown as the long-term average from 1982 to 2024 for soil profile and stream
479 water in Nemunas (W5) and Rhine (W10).

480 Generally, the magnitudes of water ages follow the geographic and climatic gradients, with younger
481 water found in catchments with higher annual precipitation inputs. Those regions locate in ~~the~~Alpine
482 regions – for instance around Alps in Southern Rhine, and in catchment W12 and W17 (Figure S6-7).
483 The north-west coast of Europe (Figure 5), particularly for Nordic catchments S5) also exhibited young
484 water age, where lower temperature and net radiation ~~further~~ limit the level of potential
485 evapotranspiration, leading to larger percolation to deeper soil layers and groundwater. Such high
486 turnover rates of water in these catchments (~~W1, W2, W3, W4, W5W6, and W8W7~~) are ~~also~~
487 demonstrated as the simulated reflected by short travel time in soil profile with average values
488 remaining below 500 days: (Table 4).

489 A similar pattern was also found in mountainous regions with higher precipitation and lower potential
490 evapotranspiration compared to lowland areas. Two clear examples are W12 and W17 located in the
491 Alps and the Taurus Mountains where water ages and travel time remained below 500 days (Table 4
492 and Figure S5-7). In specific wet periods, the soil water ages and travel time can be reduced to just
493 days, suggesting the rapid response of saturated hydrological systems ~~(e.g., the wet year 1999 in~~
494 Europe in Figure S5-7). In contrast, the lowlands in central-west Europe showed much slower
495 turnover rates, ~~with the~~. A typical example is Rhine (Figure 5), where mean water ages ~~reaching~~
496 almost reached up to 10 years in ~~some specific regions. A few examples could be~~lowlands. Such
497 phenomenon was also found in ~~the three major representative catchments in Central Europe – other~~
498 European catchment (e.g., W9 Elbe, Rhine, and W11 Danube (W9-11). Such old water ages and long
499 travel time are further exacerbated during dry years (e.g., 2004, a drought year for much of Europe
500 shown in Figure S5-7).

501 Note that though water ages and travel time share similar magnitudes and spatial patterns. It is partly
502 attributed to the fact that the travel time in the conceptualised storages increases exponentially in a
503 sequential order. Taking the Rhine as an example, the average travel time in top soil layer, median soil
504 layer, deep soil layer are 65, 225, 1291 days, respectively. Such a depth-dependence profile makes the
505 overall ages/travel time follow the magnitude of bottom layer and leads to similarity between water
506 ages and travel time. However, large discrepancies are possible between the two indices if a shallow
507 lower boundary is adopted.

508 The estimation of travel time and water ages further provides opportunities to link hydrology and
509 water quality processes in the modelling framework. The simplest and most intuitive way is to
510 compare travel times and simulated biogeochemical process kinetics. Taking denitrification as an
511 example, we applied linear regression and Spearman's correlation test to investigate the potential

512 correlation between travel time of soil water and denitrification rates. The results in [Figure 6](#) [Table 4](#)
513 showed the strong positive correlations in most agricultural-dominated catchments (W5, ~~W5~~, W6, ~~W8~~,
514 W9, [W10](#), W11, [and W13](#)) yet only weak or no [positive](#) correlation in remaining pristine watersheds.
515 This suggests that travel time might be a key control on soil nitrogen removal in European croplands.

516 More insights can be gained via examination of the Damköhler Number, which quantifies the ratio
517 between timescales of solute transport and biogeochemical transformation. Here in our modelling
518 framework, it can be calculated as the ratio between the travel time of soil water and the time for all
519 soil NO₃-N storage to be removed under the simulated denitrification rates. Damköhler numbers <1
520 mean that soil water nitrogen cannot be [fullyeffectively](#) removed during time of residence, indicating
521 the dominance of transport over removal processes and the potential of nitrogen leaching. As shown
522 in [Figure 7e6E-F](#), the long-term averages of Damköhler number remain below 1 in most croplands, [in](#)
523 [Nemunas, Rhine, and other European catchments \(Figure 6 and Figure S8\)](#), supporting the conclusion
524 from the linear regression [\(in Table 4 that](#) travel time is a major limiting factor on soil nitrogen
525 removal). Via the spatial- and temporal-explicit estimation of Damköhler number, EcoTWIN provides
526 the opportunity to bridge the catchment hydrological and water quality with travel time.

527

528 **5 Discussion**

529 **5.1 Structural and Functional Merits of EcoTWIN**

530 As a new tracer-aided ecohydrological model, EcoTWIN has novel advantages compared to previous
531 models. In this section, we briefly introduced the merits in model structure, applicability, and insights
532 from tracer-aided simulation.

533 **5.1.1 Integrated C++ framework**

534 Applications of large-scale modelling have been increasingly popular due to the accelerating
535 development of observation networks and availability of remote sensed data. However, it severely
536 increases the computational burden of ecohydrological modelling. Especially for fully distributed
537 models, increasing size of the model domain can lead to exponential increase in computation demands.
538 In this context, an integrated framework in C++ can significantly accelerate the modelling tasks, as all
539 computation can be conducted within memory thereby avoiding the additional input/output
540 overhead associated with disk-based operations in loosely coupled model chains (e.g., ECH₂O-iso-
541 nitrate; Yang et al., 2024). A standard test was not performed, but based on our modelling experience
542 in the same catchment with different models, the speed of EcoTWIN (~5 seconds for a simulation with
543 285 grid cells and 30 years at daily timestep) is close to the water quality model mHM-Nitrate (~5
544 seconds yet without isotopic simulations; Wu et al., 2022) and easily outperforms ECH₂O-iso-nitrate (7
545 minutes; Wu et al., 2025b).

546 **5.1.2 Selective disassembly structure**

547 EcoTWIN incorporates a wide range of ecohydrological processes from canopy to groundwater, which
548 not only include natural processes but also anthropogenic activities like irrigation. Land managements

549 can also be represented by dynamic parametrisation, thus enabling EcoTWIN to function as a learning
550 tool to investigate the impacts of changes in anthropogenic management over natural ecosystems;
551 for instance, the land use distribution was updated every 10 years in our test examples to reflect the
552 moderate increases in afforestation in the past 45 years in Europe. More importantly, unlike hard
553 coded process representations/equations in most ecohydrological models, EcoTWIN has a selective
554 disassembly structure, which provides alternative conceptualisations for several important hydrological
555 processes (canopy interception, percolation, groundwater recharge, as well as three pedotransfer
556 functions for initialising soil properties). Modellers can benefit from such flexible model structures by
557 either selecting process representations best suited to field knowledge or data prior to calibration, or
558 integrating module selection into the calibration thus enabling simultaneous optimisation of model
559 structure and corresponding parameters. The latter aspect, i.e., the optimisation of model structure,
560 can be realised together with the recently developed optimisation algorithm DREAM_(LOAX) that aims to
561 identify the deficits in model structure during calibration (Wu et al., 2025a).

562 ***5.1.3 Transferability to contrasting geographic and climatic contexts***

563 To thoroughly test the applicability of EcoTWIN, 17 catchments with different climatic and
564 geographical contexts were selected for calibration and validation, spanning over most biomes in
565 Europe, from snow-dominated watersheds in Nordic or alpine regions, to agricultural-influenced
566 lowlands catchments, and Mediterranean ecosystems (Figure 2 and Table 1). Through multi-criteria
567 calibration against three objectives at multiple sites, the model successfully reproduced the
568 seasonality and peaks of discharge, in-stream isotopes, and NO₃-N concentrations in most catchments.
569 Such performance is comparable or better than the previous model benchmarks at similar scales
570 (Bajracharya et al., 2023; Mikayilov et al., 2015; Rakovec et al., 2016, 2019). Note that the
571 concentration of NO₃-N was used for calibration, whose accurate simulation is more difficult than NO₃-
572 N loads given the naturally good performance in discharge. In the other words, hydrological simulation
573 is often the least problematic part in integrated water quality modelling, as it is mostly dominated by
574 natural catchment properties while nitrogen cycling is more interfered by anthropogenic
575 managements (e.g., fertilization and irrigation) (Wu et al., 2025b). Additionally, the simulated internal
576 fluxes were also compared to three reanalysis products in hydrological simulations, corresponding to
577 the key fluxes or storage states in hydrological cycling (snow melt-accumulation, evapotranspiration,
578 and water storage). The results show that constrained by isotopes, EcoTWIN was able to reproduce
579 comparable hydrological modelling results to the remote sensing data without direct calibration
580 regarding magnitudes, spatial patterns, and temporal dynamics. The only degraded performance was
581 found in GRACE surface mass anomaly in coastal regions. There are two potential reasons: (i) the
582 coarse resolution of GRACE might account for mass shifts in both ocean and land, yet EcoTWIN only
583 produces mass anomaly in terrestrial systems; (ii) bidirectional fluxes across the land-ocean interface
584 might drive key changes in coastal systems, which is not considered in current version of EcoTWIN.
585 Nonetheless, given the relatively good agreement with most available data, we conclude that
586 EcoTWIN is applicable across a range of terrestrial ecosystems from boreal to temperate and
587 subtropical climate.

588 **5.1.4 Bridging hydrology and water quality with water ages**

589 Further to the inference of hydrological and nitrogen processes that is also available in other
590 distributed water quality models (Wellen et al., 2015), a unique trait of EcoTWIN lies in its capacity to
591 track water fluxes and ages with stable water isotopes. As a tracer-aided model, EcoTWIN not only
592 simulates the celerity of catchment response, but tracks the velocity of water via different flow paths.
593 The importance of delineating flow paths within catchments has long been recognized by hydrologists,
594 and has motivated the development of many indices to describe the movement of water molecule at
595 catchment-scale and estimate associated timescales (Sprenger et al., 2019). A few examples are water
596 ages, transient time distribution, and young water fractions (Benettin et al., 2015; Hrachowitz et al.,
597 2013; Jasechko et al., 2016). However, those indices are mainly calculated in a lumped manner where
598 different flow paths in the catchment are characterised as a black box, thus characterising the overall
599 input-output dynamics yet potentially omitting important spatio-temporal variability of hydrological
600 boundary conditions. Instead, EcoTWIN, benefiting from the gridded-based structure, can utilise the
601 increasingly available spatial information (e.g., gridded remote sensing datasets) thus characterising
602 the water ages and travel time in a spatially-explicit manner. Note that simulations of water age/travel
603 time, like other ecohydrological processes, are sensitive to spatial resolution. The coarse resolution
604 used for large catchments (e.g., 5 km in this study) may obscure the sub-grid heterogeneity. For
605 instance, local hydrological hotspots characterized by short travel times and young water ages can be
606 damped or averaged out at coarser resolutions, as reported in modelling studies using Ech2O-iso
607 (Smith et al., 2021; Yang et al., 2023b). However, this limitation can be mitigated by increasing spatial
608 resolution, and it does not undermine the utility of EcoTWIN for water-tracking.

609 Compared to water age which quantifies the age of water within the overall system, travel time,
610 accounting for the water age within a specific storage, is more important in understanding the links
611 between hydrological and nutrient cycles. Such an index, also known as transit time or exposure time,
612 forms one of the fundamental components of water quality modelling. Therefore, the travel time
613 estimated by EcoTWIN has potential to improve the simulation of biogeochemical transformations in
614 water quality models interfaced with simplified hydrological modules (e.g., MONERIS; Bonchkovskiy
615 & Osadcha, 2024). Moreover, travel time can be used as a proxy to bridge hydrological processes and
616 biogeochemical transformations. Here we presented a simple framework to calculate the Damköhler
617 Number for denitrification. By using the simulated travel time and reaction timescale (i.e., the time
618 for full removal of nitrogen storage under current denitrification rates), estimation of Damköhler
619 Number was achieved in a spatially- and temporally-explicit manner (Figure 76E-F), which can
620 highlight where and when soil nitrogen removal is constrained by the limited exposure time in the
621 catchment. Such high-resolution information is unique, as the use of this index has been largely
622 restricted to steady-state groundwater systems or riparian/hyporheic zones due to the difficulty in
623 quantifying processing time and residence time at larger scales (Ocampo et al., 2006; Wu et al., 2022).

624

625 **5.2 Limitations and roadmap for future development**

626 Despite these advances, EcoTWIN has limitations. In this section, the uncertainties in model structure
627 and conceptualisation are introduced, as well as the potential roadmaps for future developments.

628 ***5.2.1 Potential towards physics-based conceptualisation of groundwater***

629 Groundwater in EcoTWIN is characterised as two conceptual storages linking with adjacent upstream
630 and downstream storages following the topographic gradients. Such conceptualisation, although has
631 been widely employed in hydrological models (e.g., SWAT, mHM, EcH₂O, STARR, etc.), does not align
632 with the physical mechanisms of groundwater routing, as groundwater flow direction follows the
633 hydraulic gradients which may not entirely coincide with topographic gradients (Condon et al., 2021).
634 Such simplified routing has less effect in large catchments with clear topographic gradients (e.g., Rhine
635 starting from Alps to North plain), yet might cause biased estimation in water mass balance for flatter
636 headwater catchments (Yang et al., 2025). Therefore, we plan to further incorporate an additional
637 groundwater module to realise physics-based routing following Darcy's Law in future.

638 ***5.2.2 Revisiting mixing strategies***

639 Mixing strategy is a key component in water quality or tracer models describing the flux-storage
640 behaviours along specific flow paths. There has long been a debate on different mixing assumptions
641 and theories. A typical example is the two-water-world hypothesis, where water storage in the soil
642 profile is differentiated into a tightly-bound pool and a mobile-water pool (McDonnell, 2014). Such
643 conceptualisation is close to the definition of soil matrix flow and preferential flow: the existence of
644 free-flowing preferential flow will bypass the soil matrix vertically and accelerate the lateral drainage
645 via direct connection with channel network (Hrachowitz et al., 2013; Sprenger et al., 2019). However,
646 a complete mixing strategy is often regarded as a reasonable first approximation in many situations
647 and is used in most water quality and tracer models (Jung et al., 2025). This is not only attributed to
648 its computational simplicity, but also the difficulty in conceptualising preferential flow in an
649 evidenced-based manner. In the other words, even with the recognition of preferential flow, its
650 calculation is often hindered by the subsurface heterogeneity in soils and bedrock; a good visualisation
651 is given in Figure 7 in Sprenger et al., (2019). Alternatively, partial mixing has been developed for
652 ecohydrological models (e.g., Hrachowitz et al., 2013), which could be added as a complementary
653 mixing strategy in EcoTWIN. However, as benchmarked in Hrachowitz et al., (2013), the partial mixing
654 brings only moderate improvements in simulations yet can introduce challenges to model spin-up (the
655 increasing instability of storage ages due to the exchange between bypass and storage compartment).
656 Moreover, the realisation of partial mixing, like preferential flow, relies on additional parameters to
657 describe the timing and extent of mixing thus introducing additional parametric uncertainty.
658 Therefore, we recommend a rigorous evaluation of the necessity of partial mixing before any
659 application.

660 **5.2.3 Complementing the in-stream biogeochemical processes**

661 Transformation is as crucial as transport in inland-water nitrogen cycling (Wang et al., 2024). In the
662 current version of EcoTWIN, denitrification is the only in-stream process of nitrogen loss. However,
663 recent studies have shown that other processes are involved which may be important for aquatic
664 nitrogen cycling. An example originates from Wang et al., (2024), where global inland-water modelling
665 shows that in-stream denitrification only accounts for a minor fraction of NO₃-N removal compared to
666 biological uptake. Though their modelling considers lakes and reservoirs where primary production of
667 benthic plants and algae is usually greater than that in rivers, in-stream assimilation might still play a
668 significant role, particularly, in slow-flowing river systems. This is supported by a recent modelling
669 study that estimated nitrogen retention at 15-min interval based on high-frequency NO₃-N data (Yang
670 et al., 2023a). Therefore, we plan to further compliment EcoTWIN with in-stream assimilation
671 conceptualisation, as well as other potentially important riverine processes (e.g., nitrogen burial in
672 sediments; Akbarzadeh et al., 2019).

673 **5.2.4 Integrated calibration framework to embrace equifinality**

674 Strictly speaking, equifinality is not specifically linked to EcoTWIN, but remains a universal problem for
675 calibration or parameter tuning for almost all ecohydrological models. It is reflected in multiple
676 parameters sets yielding similarly good model performance, thus increasing the uncertainty in process
677 inference. The extent of equifinality is primarily controlled by the magnitude of parameters and
678 observation/objectives (Wu et al., 2025c). Unfortunately, conceptualisations across diverse process
679 domains (e.g. for hydrology, isotopes and N-cycling) in EcoTWIN also lead to a relatively large number
680 of parameters. Such risk in equifinality can be potentially constrained via sensitivity analysis, but can
681 still remain an issue given the ubiquitous epistemic uncertainty in data and model structure (Beven,
682 2006, 2015). Alternatively, the recently developed calibration algorithm DREAM_(LoAx) provides an
683 opportunity to embrace equifinality by tuning parameters based on the limits-of-acceptability theory
684 under the equifinality thesis (Wu et al., 2025a). The integrated modelling framework of EcoTWIN and
685 DREAM_(LoAx) can potentially increase the robustness of model calibration and inference.

686

687 **6 Conclusions**

688 Uncertainty is a central concern in ecohydrological modelling, as models are not only used for
689 prediction of specific variables, but also for process inference (backtracking internal processes from
690 available observations) that are inherently embedded within considerable uncertainty. Stable water
691 isotopes can help effectively constrain hydrological fluxes due to their conservative nature, motivating
692 the increased development of tracer-aided models. However, few attempts have been made to
693 incorporate a tracer-aided hydrological framework into water quality models.

694 Therefore, we introduced EcoTWIN, a fully distributed tracer-aided **ecohydrological** model that **tracks**
695 **water**, **isotopic**, and **nutrient** fluxes simultaneously in an integrated C++-based framework. To
696 thoroughly validate the model, 17 large European catchments were selected with a wide range of

697 geographic and climatic gradients (from snow-dominated watersheds in Nordic or alpine regions, to
698 agricultural-influenced lowlands catchments, and Mediterranean ecosystems). The model was
699 calibrated against long-term observations of discharge, in-stream isotopes, and NO₃-N concentrations
700 during 1980-2024 in each of the 17 catchments. Additionally, uncalibrated internal states and fluxes
701 were also compared with three remote sensing products (ERA5 snow depth, MODIS
702 evapotranspiration, and GRACE surface water anomaly) to validate the credibility of process inference.

703 The generally good agreements in both calibrated in-stream components and uncalibrated internal
704 flux-states demonstrated that EcoTWIN is a transferable, flexible prediction and learning tool for
705 process inference across biomes ranging from boreal to subtropical climate. Constrained by tracer
706 simulations, the model not only reproduces the celerity of hydrological systems, but also tracks the
707 velocity. Water ages and travel time are embedded in EcoTWIN to provides spatio-temporal-explicit
708 insights into *when*, *where*, and *how* water moves in the system. Such indices further provide the
709 opportunities to efficiently bridge hydrology and water quality at large catchment-scales. An example
710 was presented using the Damköhler Number to identify regions where denitrification was limited by
711 fast turnover rates of water.

712 Following this “proof of concept” we also see numerous areas where future developments can
713 improve the limitations in the 1.0 version of the model.

714

715 **Code and data availability**

716 The initial version (v1.0) of EcoTWIN is archived in <https://doi.org/10.5281/zenodo.16747633> (Wu et
717 al., 2025d). For further development please refer to GitHub repository: [https://github.com/songjun-
718 wu/EcoTWIN](https://github.com/songjunwu/EcoTWIN). The geographic data were acquired from Catchment Characterisation and Modelling
719 database (CCM2, version 2.1). The climatic forcing was acquired from E-OBS database
720 (<https://www.ecad.eu/download/ensembles/ensembles.php>). The LAI were acquired from MODIS
721 database (<http://doi.org/10.5067/MODIS/MOD15A2H.006>). Long-term observation of discharge was
722 acquired from GRDC (<https://grdc.bafg.de/>); in-stream isotopic observations were available from
723 Wateriso database (<https://wateriso.utah.edu/waterisotopes/index.html>) and GNIR database
724 (<https://www.iaea.org/services/networks/gnir>); In-stream NO₃-N concentration were acquired from
725 global water quality database, GEMStat (<https://gemstat.org/>).

726

727 **Acknowledgements**

728 Tetzlaff's and Wu's contributions were partly funded through the WETSCAPES2.0 project (DFG
729 TRR410/1 2025) and the Einstein Research Unit “Climate and Water under Change” from the Einstein
730 Foundation Berlin and Berlin University Alliance (grant no. ERU-2020-609). Tetzlaff was also partly
731 funded through Leibniz Excellence project ISOSCALE and received funding from the
732 “Wasserressourcenpreis 2024” of the Rüdiger Kurt Bode-Foundation. This research was also
733 supported by the BMBF (funding code 033W034A), which supported the IGB stable isotope Laboratory.

734 Contributions from Soulsby were supported by Leibnitz Association Germany in the project Wetland
735 Restoration in Peatlands.

736

737 **Author contribution**

738 Conceptualization: SW, DT, YZ, CS

739 Data curation: SW

740 Methodology: SW

741 Software: SW

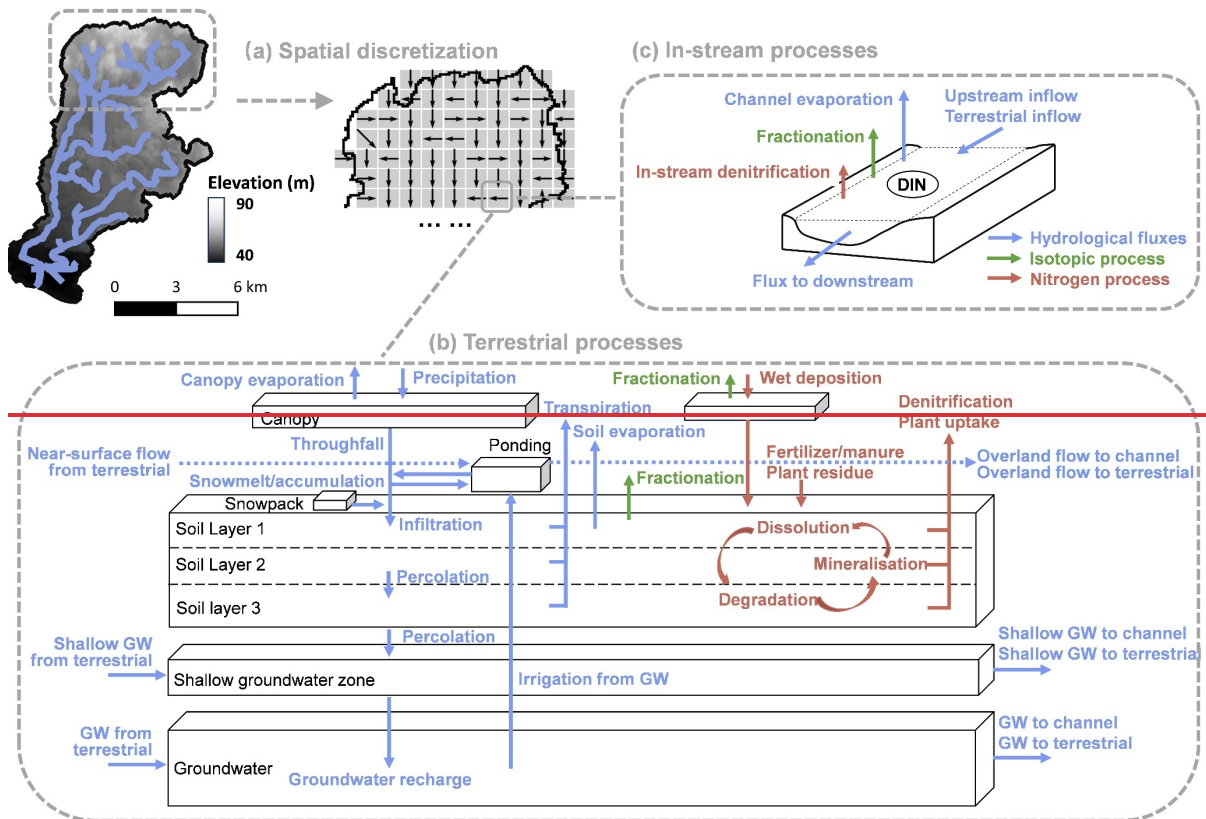
742 Investigation: SW, DT, YZ, CS

743 Visualization: SW

744 Supervision: DT, CS

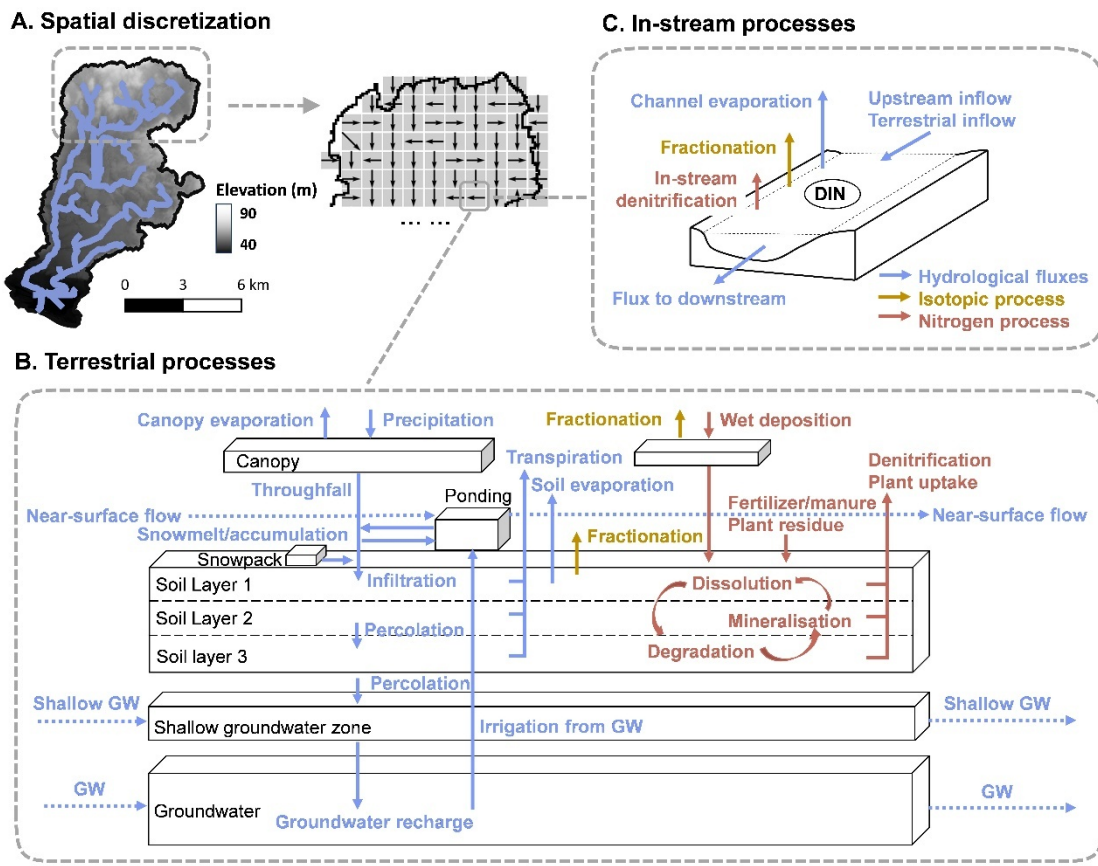
745 Writing (original draft preparation): SW

746 Writing (review and editing): SW, DT, YZ, CS



748

749 **Figure 1. Model structure of EcoTWIN. As a distributed model, EcoTWIN disentangles the spatial**
 750 **domain into grid cells (Panel a). In each grid cell, hydrological, isotopic, and nitrogen processes were**
 751 **simulated in canopy, snow, soils, shallow groundwater, and groundwater (panel b) and river channel**
 752 **if channels are present (Panel c).**



753

754

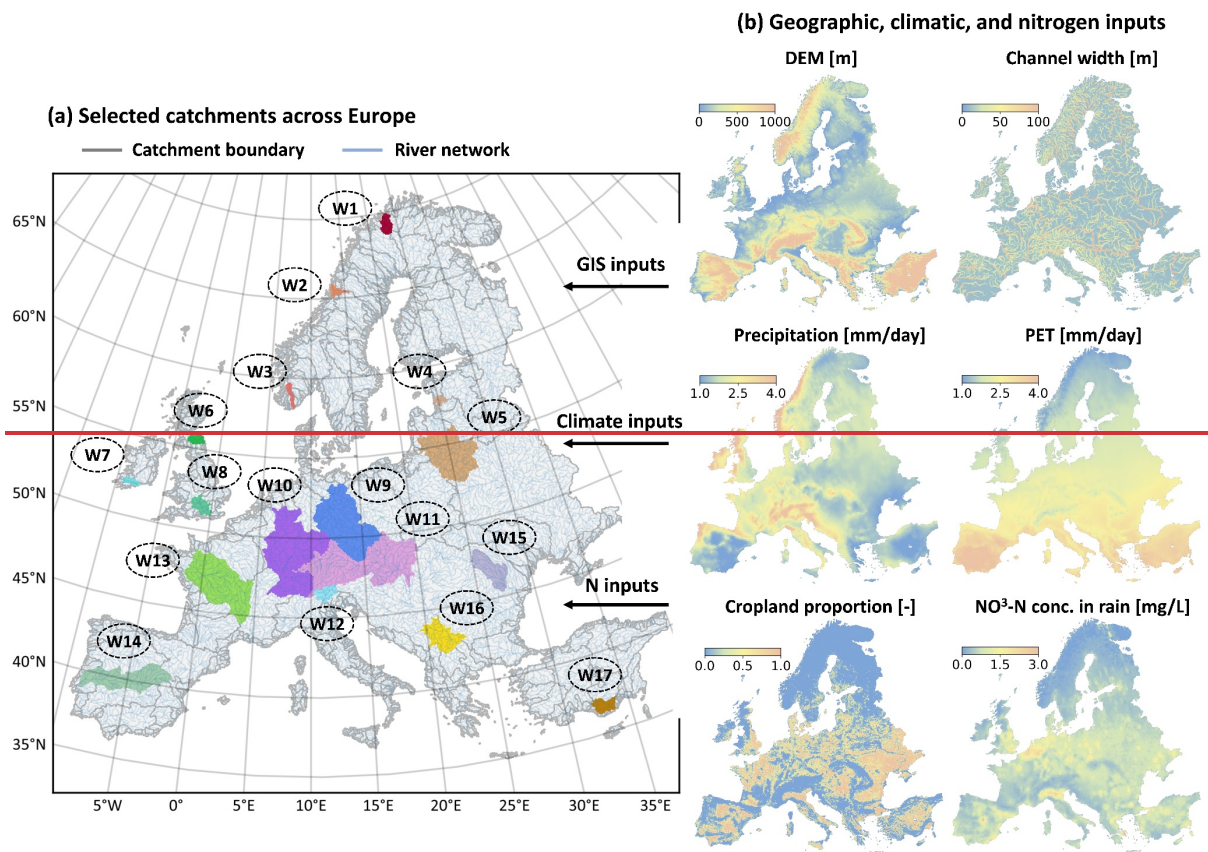
755

756

757

758

Figure 1. Model structure of EcoTWIN. As a distributed model, EcoTWIN disentangles the spatial domain into grid cells (Panel A). In each grid cell, hydrological, isotopic, and nitrogen processes were simulated in canopy, snow, soils, shallow groundwater, and groundwater (Panel B) and river channel if channels are present (Panel C).

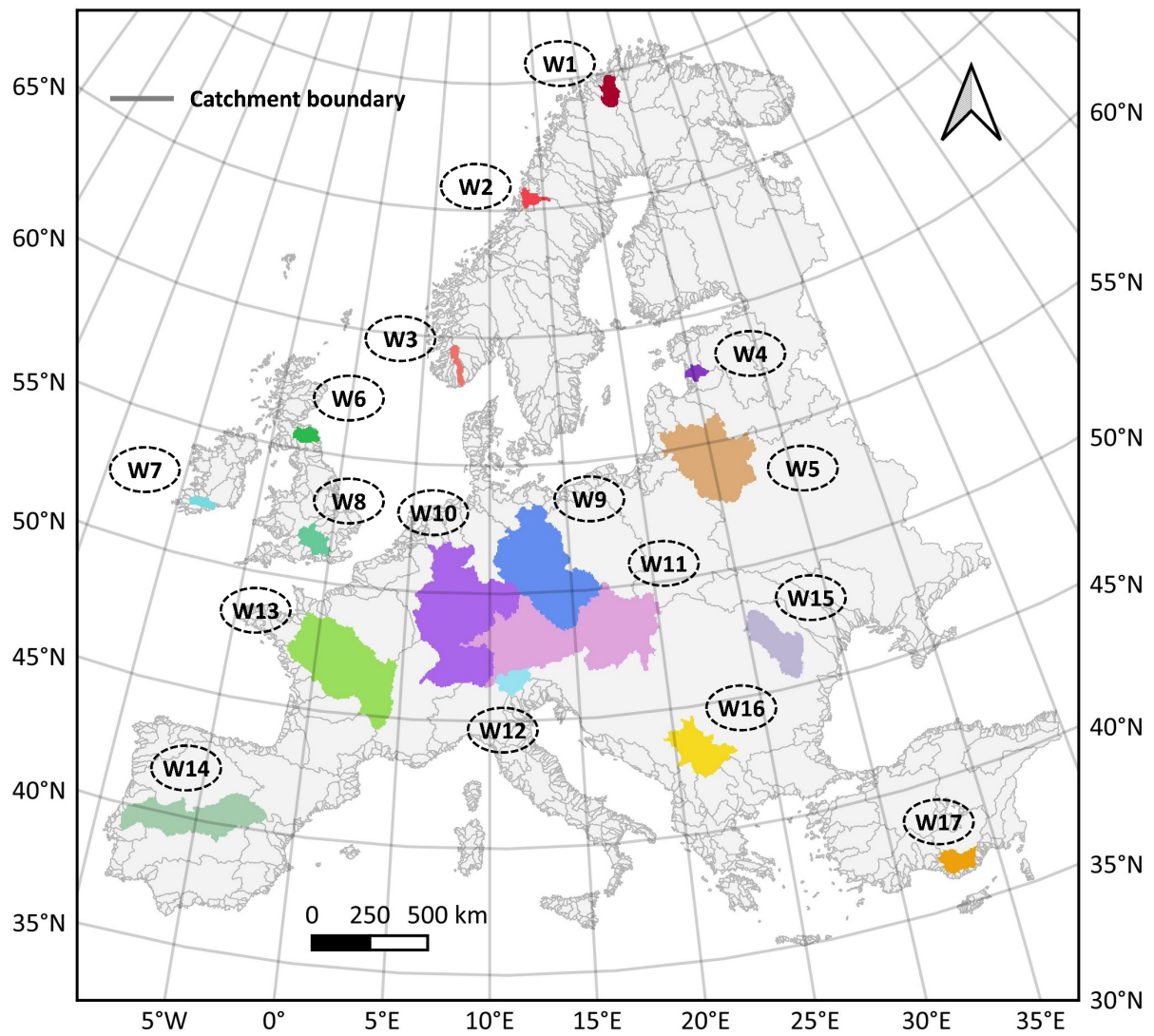


760

761

762

Figure 2. The selected catchments for model validation (Panel a) and an overview of key geographic, climatic, and nitrogen inputs (Panel b).

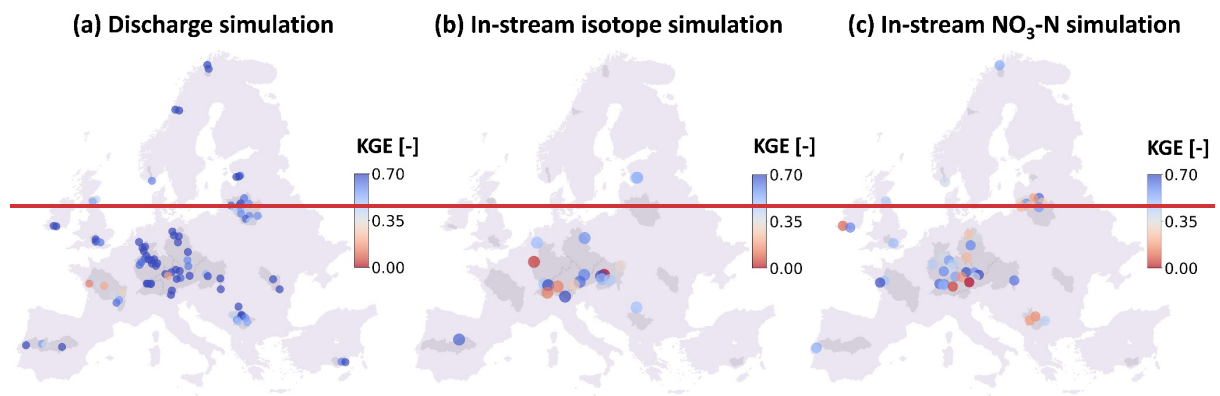


763

764 Figure 2. The selected catchments for model calibration and validation. The overview of key
 765 geographic, climatic, and nitrogen inputs are show in Figure S1.

766

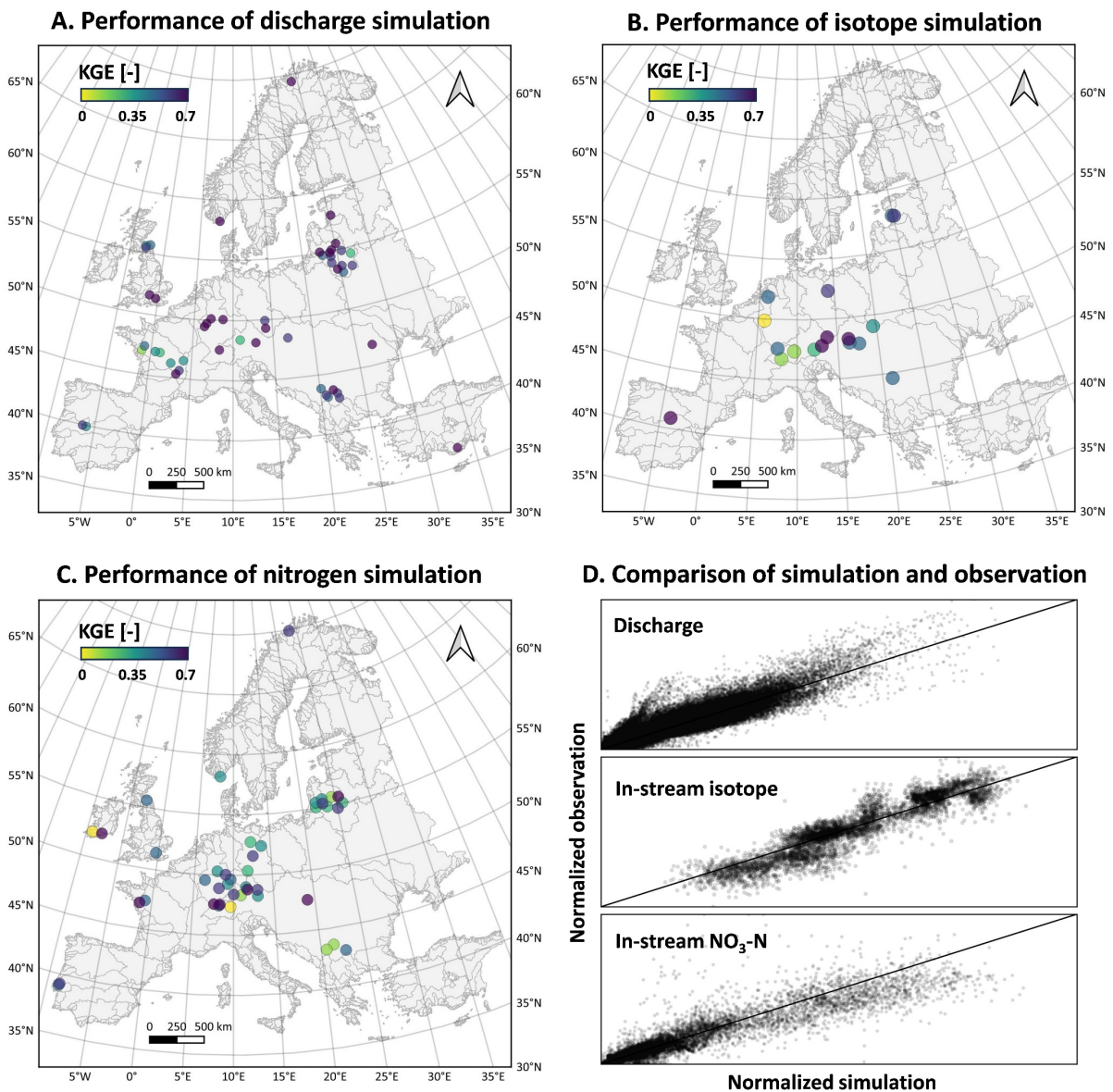
767



768

769 ~~Figure 3. The simulation performance of discharge, in stream isotope, and in stream NO₃-N. The~~
770 ~~simulated and observed time series are shown in Figure S1.~~

771



772

773

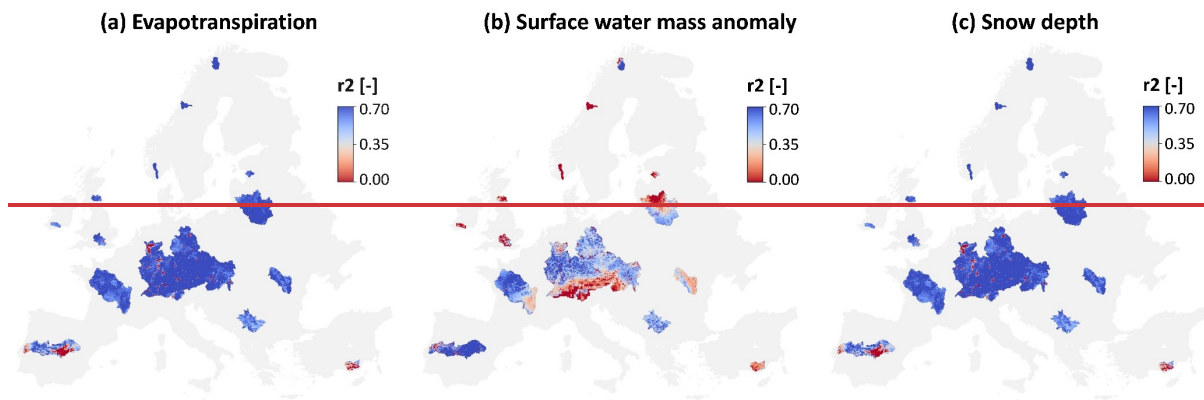
774

775

776

777

Figure 3. The simulation performance of discharge (A), in-stream isotope (B), and in-stream NO₃-N (C) evaluated using KGE. The comparison between simulation and observation values are shown in Panel D. Catchment-specific performances are summarised in KGE, RMSE, Pearson correlation coefficient, and Pbias in Table 2.



778

779

780

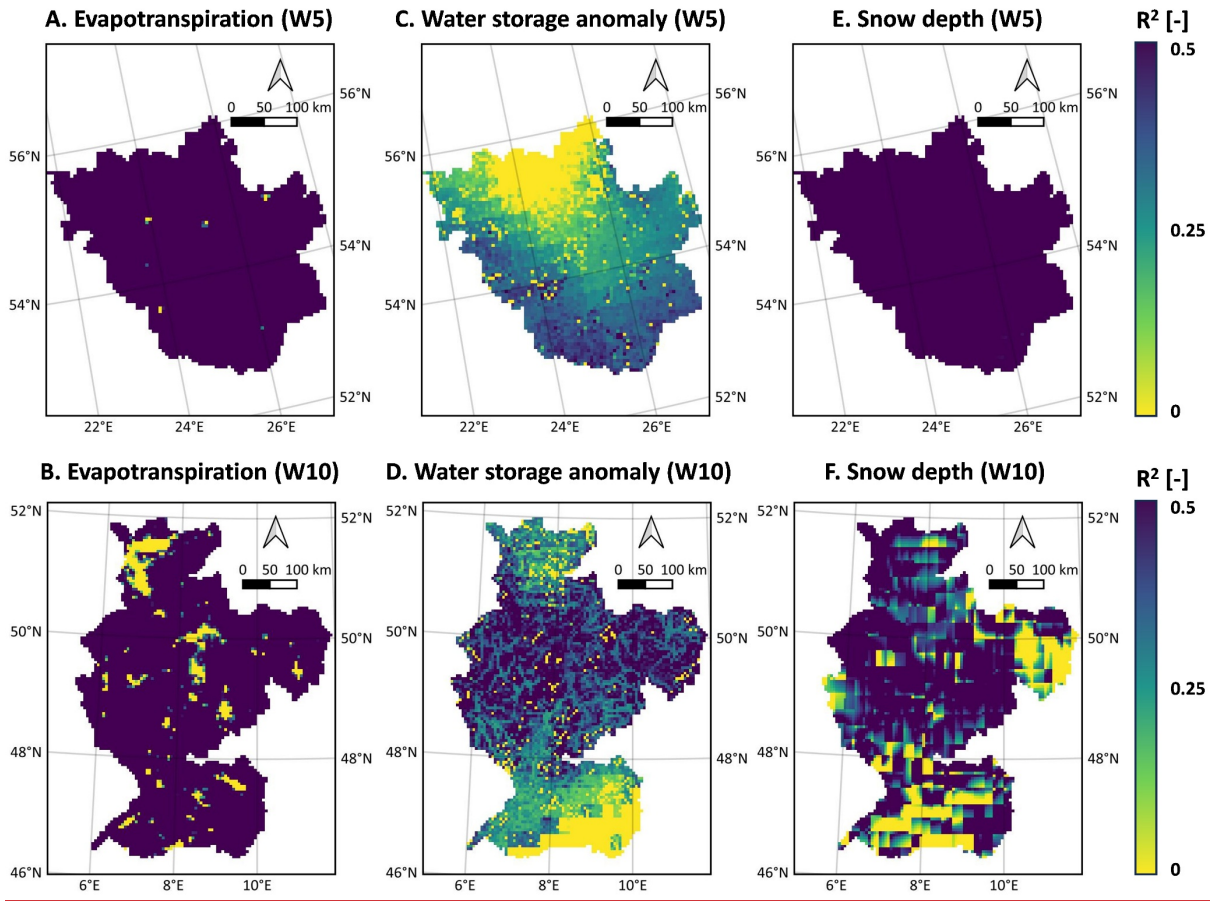
781

782

783

784

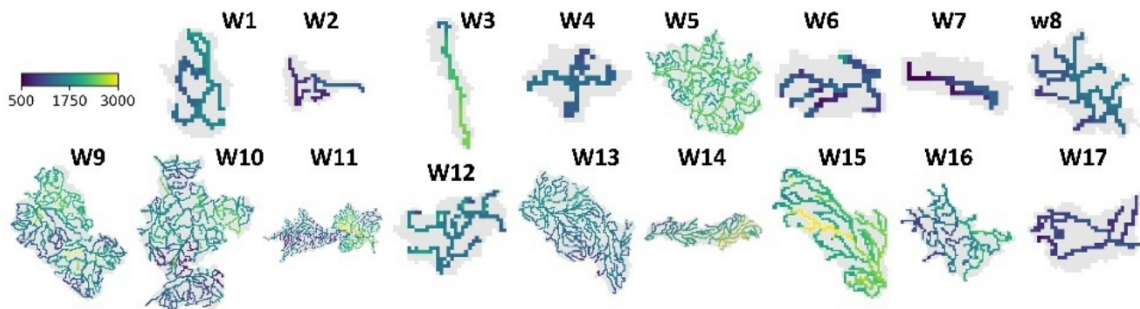
Figure 4. The grid-to-grid comparison between time-series of simulated internal states/fluxes and the ones extracted from remote sensing/reanalysis products, including evapotranspiration from MODIS (Panel a), surface water mass anomaly from GRACE (Panel b), and snow depth from ERA5 (Panel c). The time-series of simulation and remote sensing/reanalysis products in each catchment are shown Figure S2-4.



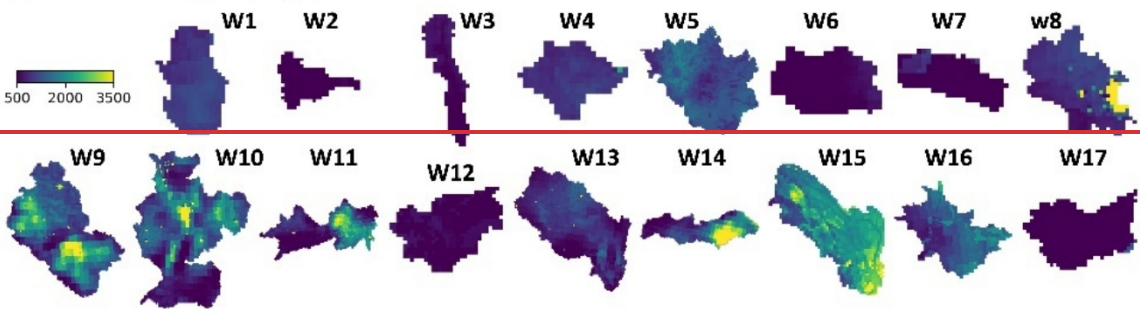
785

786 Figure 4. The grid-to-grid comparison (in coefficient of determination R^2) between time series of
 787 simulated internal states/fluxes and the corresponding records extracted from remote
 788 sensing/reanalysis products, including evapotranspiration from MODIS (Panel A-B), surface water
 789 mass anomaly from GRACE (Panel C-D), and snow depth from ERA5 (Panel E-F). The validation of two
 790 representative catchments is shown here (W5 Nemunas and W10 Rhine), while the spatial maps of all
 791 catchments were shown in Figure S2-4. The evaluation metrics in each catchment were summarised
 792 in Table 3.

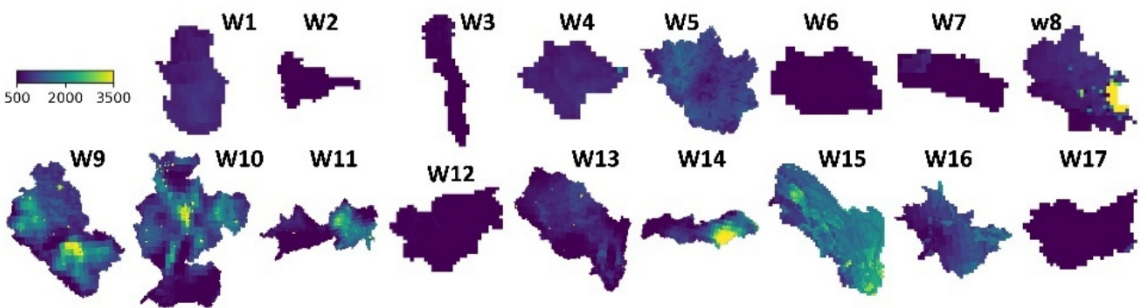
(a) Stream water age [days]



(b) Soil water ages [days]



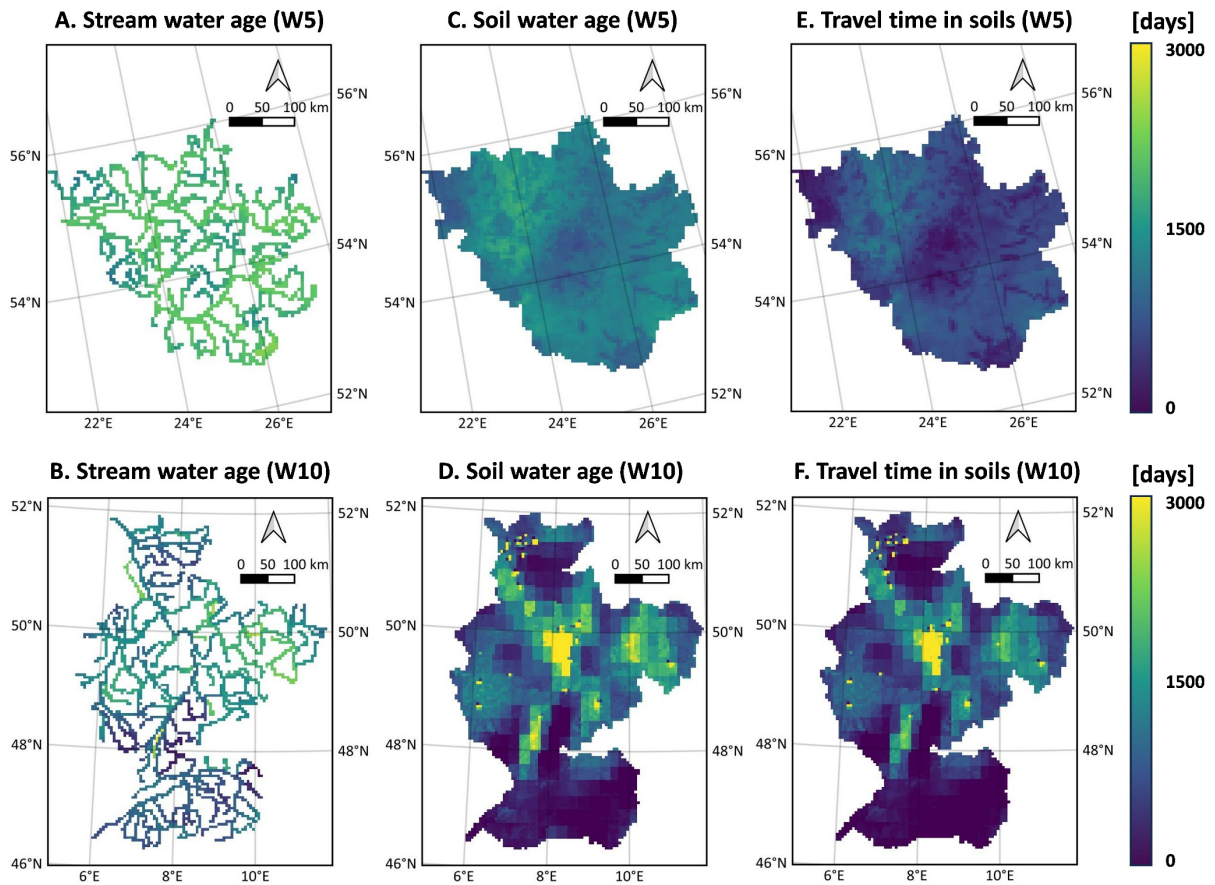
(c) Travel time in soils [days]



794

795 Figure 5. The simulated long-term average (1982–2024) of water age and travel time in channel and
 796 soil profile. Water ages represent the time since water enters the catchments as precipitation, while
 797 travel times depict the residence time of water within the specific storage.

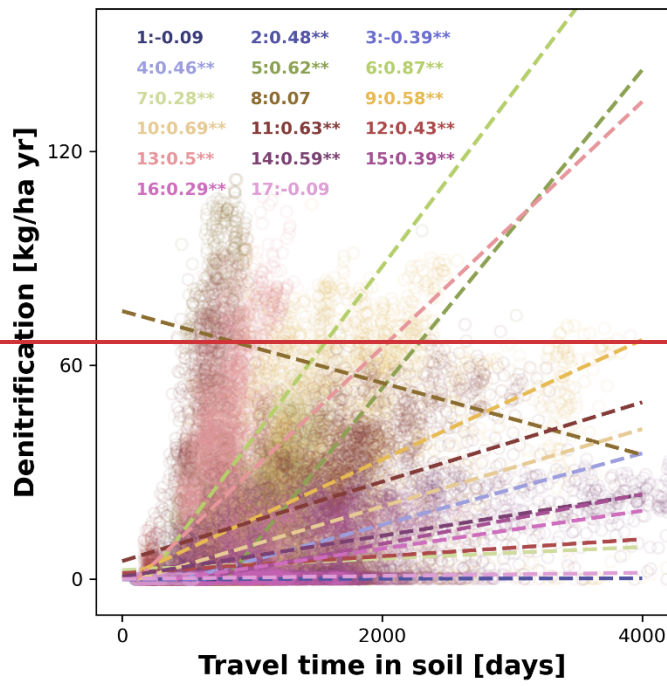
798



799

800 Figure 5. The simulated long-term average (1982-2024) of stream water age (Panel A-B), soil water
 801 age (Panel C-D), and travel time of soil water (Panel E-F). Water age represents the time since water
 802 enters the catchments as precipitation, while travel time depicts the residence time of water within
 803 the specific storage (i.e., the soil profile in this figure).

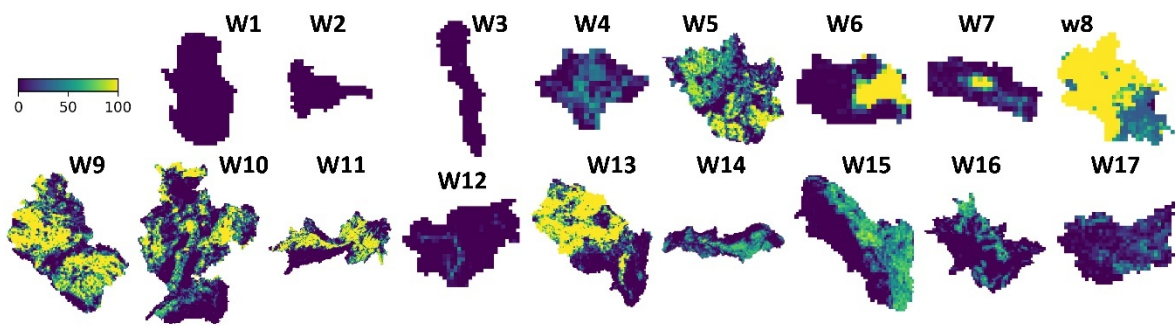
804



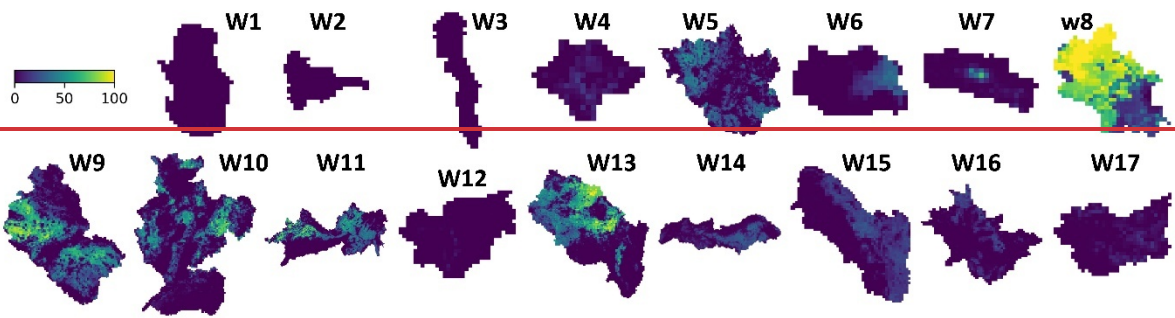
805
806
807
808
809

Figure 6. The correlations between travel time and annual denitrification. The text depicts the spearman correlation coefficients and p values (* = less than 0.05, ** = less than 0.01) in each catchment.

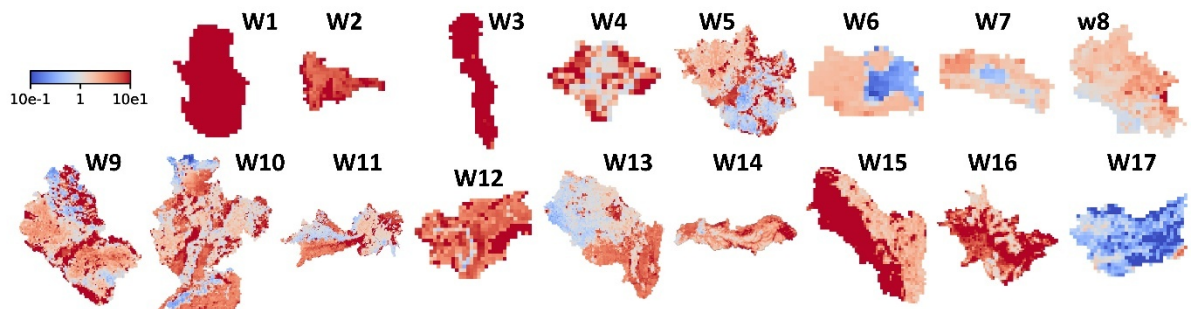
(a) Nitrogen inputs [kg/ha yr]



(b) Soil denitrification [kg/ha yr]



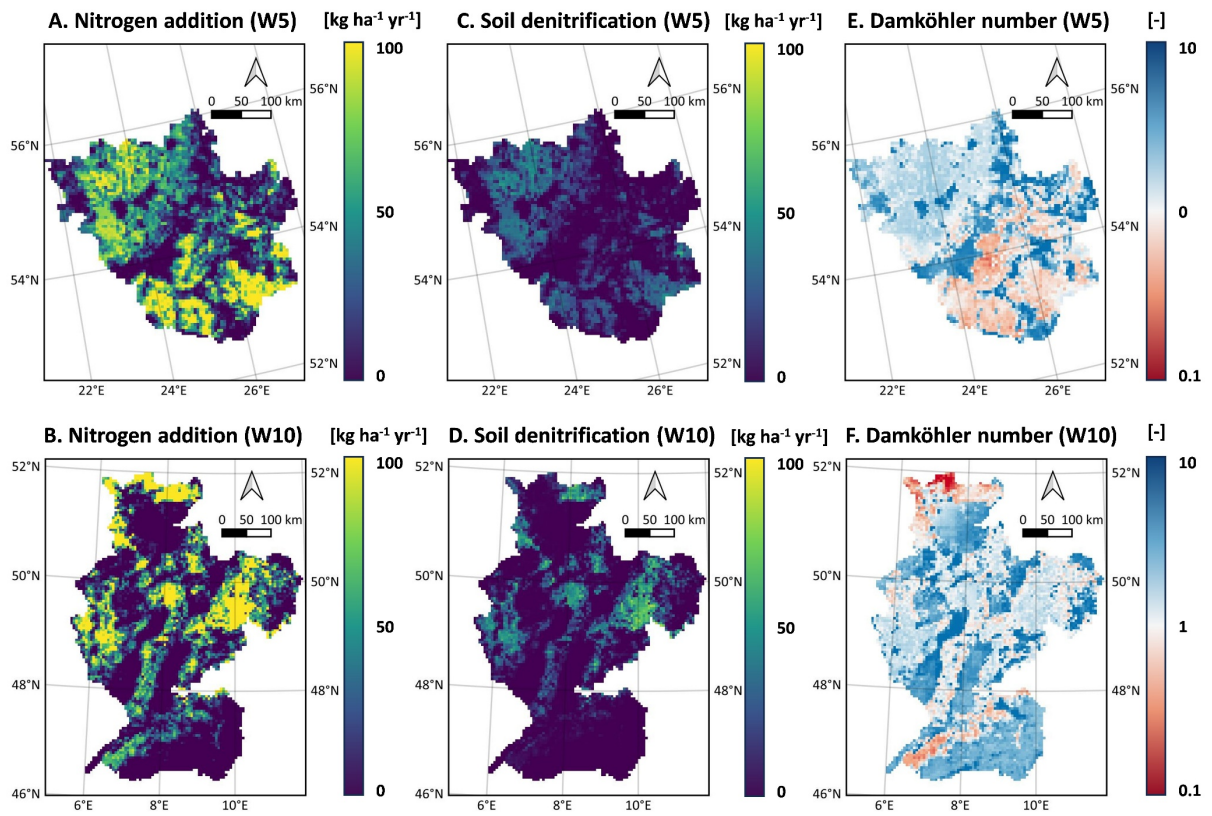
(c) Damköhler number [-]



810

811 Figure 7. The simulated long-term average (1982-2024) of nitrogen inputs, soil denitrification, and
812 Damköhler number.

813



814

815

816

817

818

Figure 6. The simulated long-term average (1982-2024) of nitrogen addition from fertilization (Panel A-B), soil denitrification (Panel C-D), and Damköhler number (Panel E-F). Note that logarithmic scale is used for Damköhler number.

819

820 **Tables**

821 Table 1. Characteristics of the selected catchments. **Lat** depicts the latitude of upper left corner of the
 822 catchment. **DEM** and **Area** are the mean elevation in m.a.s.l. and catchment size in km². **Precip**, **Temp**,
 823 and **PET** are the annual averages of precipitation, air temperature, and potential evapotranspiration
 824 in mm/yr. f_{crop} , f_{forest} , and f_{urban} are the fractions of cropland, forest, and urbanized areas in 2019
 825 in %. Null means no name is assigned for the catchment in the Catchment Characterisation and
 826 Modelling (CCM) database.

ID	Name	Lat	Area	DEM	Precip	Temp	PET	f_{crop}	f_{forest}	f_{urban}
1	Null	70.0	8725	468.5	448.5	-1.8	442.8	<1	1.9	<1
2	Vefsna	65.9	5475	636.5	1260.8	0.7	433.6	<1	24.6	<1
3	Null	59.8	5225	742.3	1400.9	3.0	545.7	<1	39.8	<1
4	Null	58.3	4350	67.4	654.5	6.4	667.9	17.4	60.5	1.4
5	Nemunas	56.6	97550	147.9	599.3	7.1	730.6	33.0	39.1	4.5
6	Tweed	55.9	6250	264.3	1023.4	7.9	600.9	21.8	18.9	1.4
7	Null	52.3	4300	175.4	1218.1	10.1	645.2	12.1	17.4	1.9
8	Thames	52.2	11900	112.0	700.7	10.4	782.9	44.9	14.1	22.0
9	Elbe	53.5	130225	318.3	626.9	8.8	836.3	41.2	34.6	10.8
10	Rhine	52.0	170175	508.3	943.3	8.9	821.0	21.5	41.2	17.1
11	Danube _(a)	50.5	197600	618.0	843.6	8.3	857.4	28.5	37.1	11.5
12	Adige	47.2	11600	1771.9	1002.3	4.5	809.7	<1	48.8	3.2
13	Loire	48.7	122125	298.9	778.7	11.0	887.4	37.6	25.7	6.5
14	Tajo	40.4	75575	686.2	549.5	14.3	1359.6	26.7	34.5	3.3
15	Danube _(b)	48.4	37975	533.3	534.7	8.1	869.5	32.0	41.3	6.4
16	Danube _(c)	44.8	37725	653.3	684.7	9.7	994.2	12.8	44.3	5.8
17	Null	37.6	12650	1384.5	454.1	12.2	1256.9	5.9	4.3	<1

827

828

829 Table 2. The calibration performance of discharge (Q), in-stream isotopes (¹⁸O, Iso), and nitrate (NO³-
 830 N). Evaluation metrics include Kling-Gupta efficiency (-), Root Mean Square Error (m³/s, ‰, and mg/L
 831 for discharge, isotopes, and nitrate, respectively), Pearson Correlation Coefficient (-), and Percent bias
 832 (%).

Metric	Unit	Min	Max	Mean	Median
Kling-Gupta efficiency (Q)	-	0.14	0.89	0.65	0.69
Kling-Gupta efficiency (Iso)	-	-0.03	0.86	0.45	0.48
Kling-Gupta efficiency (NO ³ -N)	-	-0.36	0.72	0.42	0.44
Pearson correlation coefficient (Q)	-	0.49	0.92	0.79	0.81
Pearson correlation coefficient (Iso)	-	0.14	0.87	0.51	0.54
Pearson correlation coefficient (NO ³ -N)	-	-0.26	0.86	0.55	0.6
Root Mean Square Error (Q)	m ³ /s	3.99	677.08	123.02	68.51
Root Mean Square Error (Iso)	‰	0.31	1.51	0.72	0.73
Root Mean Square Error (NO ³ -N)	mg/L	0.02	2.82	0.83	0.57
Percent bias (Q)	%	0.52	79.88	17.44	9.53
Percent bias (Iso)	%	-11.28	-0.07	-4.3	-4.42
Percent bias (NO ³ -N)	%	0.18	49.25	15.52	10.89

833

834 Table 2. Calibration statistics for discharge (*q*), in-stream isotope (*iso*), and in-stream NO₃-N (*no3*)
 835 across the 17 selected catchments. Evaluation metrics represent the mean values computed within
 836 each catchment.

ID	Number of sites			Kling-Gupta efficiency			Pearson Correlation			Root Mean Square Error			Percent bias		
	<i>q</i>	<i>iso</i>	<i>no3</i>	<i>q</i>	<i>iso</i>	<i>no3</i>	<i>q</i>	<i>iso</i>	<i>no3</i>	<i>q</i>	<i>iso</i>	<i>no3</i>	<i>q</i>	<i>iso</i>	<i>no3</i>
	-	-	-	-	-	-	-	-	-	m ³ /s	‰	mg/L	%	%	%
W1	2	0	1	0.7		0.5	0.9		0.6	56		0.0	16.4		0.2
W2	2	0	0	0.9			0.9			47			3.3		
W3	1	0	1	0.6		0.4	0.7		0.4	62		0.0	22.5		2.3
W4	3	2	0	0.7	0.5		0.7	0.5		12	0.8		9.5	2.5	
W5	13	0	9	0.6		0.4	0.6		0.6	64		1.4	15.8		22.2
W6	3	0	1	0.4		0.4	0.9		0.4	42		0.4	48.3		4.3
W7	2	0	2	0.8		0.4	0.9		0.5	22		0.5	3.6		18.8
W8	3	0	1	0.7		0.5	0.9		0.5	18		1.3	17.0		6.6
W9	7	1	4	0.7	0.6	0.4	0.8	0.7	0.5	114	0.7	0.9	8.1	6.3	21.5
W10	18	6	10	0.8	0.3	0.5	0.9	0.4	0.6	232	0.8	0.8	8.0	5.4	13.7
W11	12	8	9	0.7	0.4	0.4	0.8	0.5	0.5	231	0.6	0.6	15.6	3.1	19.3
W12	2	1	0	0.8	0.9		0.8	0.9		43	0.3		2.5	0.9	
W13	8	0	2	0.4		0.6	0.8		0.6	120		1.1	52.9		14.1
W14	4	1	2	0.6	0.7	0.5	0.7	0.7	0.6	107	0.8	0.3	23.7	5.5	5.9
W15	2	0	0	0.7			0.8			113			5.8		
W16	9	1	3	0.6	0.5	0.3	0.7	0.5	0.4	59	1.5	0.5	20.4	-	3.7
W17	2	0	0	0.7			0.7			56			8.4		

837

838

839 Table 3. Validation performance of evapotranspiration (against MODIS records), water storage
 840 anomaly (against GRACE records), and snow depth (against ERA5 records). Performance is evaluated
 841 using the mean Kling–Gupta efficiency (KGE), Pearson correlation coefficient (r), root mean square
 842 error (RMSE), and percent bias (Pbias) across all grid cells within each of the 17 catchments.

<u>ID</u>	<u>Evapotranspiration</u>				<u>Water storage anomaly</u>				<u>Snow depth</u>			
	<u>KGE</u>	<u>r</u>	<u>RMSE</u>	<u>Pbias</u>	<u>KGE</u>	<u>r</u>	<u>RMSE</u>	<u>Pbias</u>	<u>KGE</u>	<u>r</u>	<u>RMSE</u>	<u>Pbias</u>
	<u>-</u>	<u>-</u>	<u>m</u>	<u>-</u>	<u>-</u>	<u>-</u>	<u>m</u>	<u>-</u>	<u>-</u>	<u>-</u>	<u>m</u>	<u>-</u>
<u>W1</u>	<u>0.88</u>	<u>0.95</u>	<u>0.00</u>	<u>0.3</u>	<u>-</u>	<u>0.79</u>	<u>0.03</u>	<u>8.7</u>	<u>0.78</u>	<u>0.90</u>	<u>0.04</u>	<u>57.5</u>
<u>W2</u>	<u>0.79</u>	<u>0.96</u>	<u>0.00</u>	<u>0.2</u>	<u>-</u>	<u>0.77</u>	<u>0.14</u>	<u>37.5</u>	<u>0.19</u>	<u>0.81</u>	<u>0.12</u>	<u>162.5</u>
<u>W3</u>	<u>0.80</u>	<u>0.94</u>	<u>0.00</u>	<u>0.3</u>	<u>-</u>	<u>0.45</u>	<u>0.08</u>	<u>18.5</u>	<u>0.65</u>	<u>0.82</u>	<u>0.06</u>	<u>1159.7</u>
<u>W4</u>	<u>0.67</u>	<u>0.88</u>	<u>0.00</u>	<u>0.3</u>	<u>-</u>	<u>0.51</u>	<u>0.05</u>	<u>13.1</u>	<u>0.52</u>	<u>0.85</u>	<u>0.01</u>	<u>14.6</u>
<u>W5</u>	<u>0.70</u>	<u>0.88</u>	<u>0.00</u>	<u>0.3</u>	<u>-</u>	<u>0.49</u>	<u>0.05</u>	<u>258.6</u>	<u>0.81</u>	<u>0.90</u>	<u>0.01</u>	<u>99.9</u>
<u>W6</u>	<u>0.65</u>	<u>0.90</u>	<u>0.00</u>	<u>0.3</u>	<u>-</u>	<u>0.46</u>	<u>0.03</u>	<u>18.4</u>	<u>0.40</u>	<u>0.82</u>	<u>0.00</u>	<u>1.9</u>
<u>W7</u>	<u>0.60</u>	<u>0.91</u>	<u>0.00</u>	<u>0.2</u>	<u>-</u>	<u>0.46</u>	<u>0.03</u>	<u>10.0</u>	<u>0.07</u>	<u>0.67</u>	<u>0.00</u>	<u>46.3</u>
<u>W8</u>	<u>0.58</u>	<u>0.89</u>	<u>0.00</u>	<u>0.4</u>	<u>-</u>	<u>0.65</u>	<u>0.03</u>	<u>8.3</u>	<u>0.28</u>	<u>0.81</u>	<u>0.00</u>	<u>10.7</u>
<u>W9</u>	<u>0.08</u>	<u>0.86</u>	<u>0.00</u>	<u>0.9</u>	<u>-</u>	<u>0.59</u>	<u>0.04</u>	<u>4.0</u>	<u>0.65</u>	<u>0.82</u>	<u>0.01</u>	<u>28.0</u>
<u>W10</u>	<u>0.44</u>	<u>0.90</u>	<u>0.00</u>	<u>0.6</u>	<u>-</u>	<u>0.62</u>	<u>0.05</u>	<u>4.7</u>	<u>0.25</u>	<u>0.78</u>	<u>0.03</u>	<u>8021.9</u>
<u>W11</u>	<u>0.39</u>	<u>0.90</u>	<u>0.00</u>	<u>0.6</u>	<u>-</u>	<u>0.53</u>	<u>0.05</u>	<u>4.3</u>	<u>0.36</u>	<u>0.80</u>	<u>0.02</u>	<u>99.4</u>
<u>W12</u>	<u>0.65</u>	<u>0.92</u>	<u>0.00</u>	<u>0.3</u>	<u>-</u>	<u>0.57</u>	<u>0.07</u>	<u>14.0</u>	<u>0.54</u>	<u>0.73</u>	<u>0.07</u>	<u>125.8</u>
<u>W13</u>	<u>0.67</u>	<u>0.90</u>	<u>0.00</u>	<u>0.3</u>	<u>-</u>	<u>0.64</u>	<u>0.04</u>	<u>3.2</u>	<u>0.62</u>	<u>0.78</u>	<u>0.00</u>	<u>434.3</u>
<u>W14</u>	<u>0.35</u>	<u>0.60</u>	<u>0.00</u>	<u>0.7</u>	<u>-</u>	<u>0.74</u>	<u>0.03</u>	<u>5.2</u>	<u>0.06</u>	<u>0.66</u>	<u>0.00</u>	<u>158.1</u>
<u>W15</u>	<u>0.67</u>	<u>0.90</u>	<u>0.00</u>	<u>0.3</u>	<u>-</u>	<u>0.50</u>	<u>0.06</u>	<u>2.5</u>	<u>0.16</u>	<u>0.79</u>	<u>0.01</u>	<u>536.2</u>
<u>W16</u>	<u>0.59</u>	<u>0.82</u>	<u>0.00</u>	<u>0.3</u>	<u>-</u>	<u>0.65</u>	<u>0.05</u>	<u>2.2</u>	<u>0.21</u>	<u>0.81</u>	<u>0.01</u>	<u>18.6</u>
<u>W17</u>	<u>0.18</u>	<u>0.78</u>	<u>0.00</u>	<u>0.4</u>	<u>-</u>	<u>0.43</u>	<u>0.06</u>	<u>4.3</u>	<u>-0.05</u>	<u>0.78</u>	<u>0.02</u>	<u>62.4</u>

843

844 Table 4. Mean soil travel time and soil denitrification in selected catchments during 1982–2024. The
 845 regression slope of the fitted relationship between soil travel time and denitrification, along with the
 846 P-values of the Spearman test, are also reported.

<u>ID</u>	<u>Avg. Soil travel time</u> <u>[days]</u>	<u>Soil denitrification</u> <u>[kg ha⁻¹]</u>	<u>Slope</u> <u>[-]</u>	<u>P-value</u> <u>[-]</u>
<u>W1</u>	<u>808.56</u>	<u>0.01</u>	<u>-0.01</u>	<u><0.05</u>
<u>W2</u>	<u>206.20</u>	<u>0.01</u>	<u>0.07</u>	<u><0.05</u>
<u>W3</u>	<u>434.02</u>	<u>0.01</u>	<u>0.00</u>	<u><0.05</u>
<u>W4</u>	<u>804.22</u>	<u>3.33</u>	<u>10.01</u>	<u><0.05</u>
<u>W5</u>	<u>1067.89</u>	<u>11.98</u>	<u>44.63</u>	<u><0.05</u>
<u>W6</u>	<u>296.05</u>	<u>5.02</u>	<u>48.53</u>	<u><0.05</u>
<u>W7</u>	<u>388.63</u>	<u>3.19</u>	<u>1.62</u>	<u><0.05</u>
<u>W8</u>	<u>1063.87</u>	<u>64.50</u>	<u>-10.08</u>	<u>0.12</u>
<u>W9</u>	<u>1279.90</u>	<u>21.51</u>	<u>16.77</u>	<u><0.05</u>
<u>W10</u>	<u>1099.18</u>	<u>10.64</u>	<u>10.86</u>	<u><0.05</u>
<u>W11</u>	<u>948.22</u>	<u>15.64</u>	<u>11.14</u>	<u><0.05</u>
<u>W12</u>	<u>320.98</u>	<u>0.21</u>	<u>0.43</u>	<u>0.06</u>
<u>W13</u>	<u>719.82</u>	<u>20.88</u>	<u>34.47</u>	<u><0.05</u>
<u>W14</u>	<u>1336.50</u>	<u>8.40</u>	<u>5.76</u>	<u><0.05</u>
<u>W15</u>	<u>1681.02</u>	<u>7.72</u>	<u>6.96</u>	<u><0.05</u>
<u>W16</u>	<u>1039.28</u>	<u>3.46</u>	<u>5.32</u>	<u><0.05</u>
<u>W17</u>	<u>419.38</u>	<u>2.22</u>	<u>2.38</u>	<u><0.05</u>

847

848 **Reference**

- 849 Akbarzadeh, Z., Maavara, T., Slowinski, S., & Van Cappellen, P. (2019). Effects of Damming on River
850 Nitrogen Fluxes: A Global Analysis. *Global Biogeochemical Cycles*, 33.
851 <https://doi.org/10.1029/2019GB006222>
- 852 Ala-aho, P., Tetzlaff, D., Mcnamara, J., Laudon, H., & Kormos, P. (2017). Modeling the isotopic
853 evolution of snowpack and snowmelt: Testing a spatially distributed parsimonious approach.
854 *Water Resources Research*, 53. <https://doi.org/10.1002/2017WR020650>
- 855 Amato, M. T., & Giménez, D. (2024). Predicting monthly near-surface soil temperature from air
856 temperature and the leaf area index. *Agricultural and Forest Meteorology*, 345, 109838.
857 <https://doi.org/10.1016/j.agrformet.2023.109838>
- 858 Arnold, J., Moriasi, D., Gassman, P., Abbaspour, K., White, M., Srinivasan, R., et al. (2012). SWAT:
859 Model use, calibration, and validation. *Transactions of the ASABE (American Society of*
860 *Agricultural and Biological Engineers)*, 55. <https://doi.org/10.13031/2013.42256>
- 861 Bajracharya, A., Moghairib, M., Stadyk, T., & Asadzadeh, M. (2023). Process based calibration of a
862 continental-scale hydrological model using soil moisture and streamflow data. *Journal of*
863 *Hydrology: Regional Studies*, 47, 101391. <https://doi.org/10.1016/j.ejrh.2023.101391>
- 864 Benettin, P., Bailey, S., Campbell, J., Green, M., Rinaldo, A., Likens, G., et al. (2015). Linking water age
865 and solute dynamics in streamflow at the Hubbard Brook Experimental Forest, NH, USA.
866 *Water Resources Research*, 51, 9256–9272. <https://doi.org/10.1002/2015WR017552>
- 867 Beven, K. (2006). A manifesto for the equifinality thesis. *Journal of Hydrology*, 320(1–2), 18–36.
868 <https://doi.org/10.1016/J.JHYDROL.2005.07.007>
- 869 Beven, K. (2015). Facets of uncertainty: Epistemic uncertainty, non-stationarity, likelihood, hypothesis
870 testing, and communication. *Hydrological Sciences Journal*, 61, 150407155940006.
871 <https://doi.org/10.1080/02626667.2015.1031761>
- 872 Birkel, C., & Soulsby, C. (2015). Advancing tracer-aided rainfall-runoff modelling: A review of progress,
873 problems and unrealised potential. *Hydrological Processes*, 29(25), 5227–5240.
874 <https://doi.org/10.1002/HYP.10594>
- 875 Birkel, C., Tetzlaff, D., & Dunn, S. (2011). Using time domain and geographic source tracers to
876 conceptualize streamflow generation processes in lumped rainfall-runoff models. *Water*
877 *Resources Research - WATER RESOUR RES*, 47. <https://doi.org/10.1029/2010WR009547>
- 878 Bonchkovskiy, A., & Osadcha, N. (2024). Modelling of the nutrient load in the Sula River basin using
879 the MONERIS. *Physical Geography and Geomorphology*, 47, 7–20.
880 <https://doi.org/10.17721/phgg.2024.3-4.01>
- 881 Condon, L., Kollet, S., Bierkens, M., Maxwell, R., Hill, M., Franssen, H.-J., et al. (2021). Global
882 Groundwater Modeling and Monitoring: Opportunities and Challenges. *Water Resources*
883 *Research*, 57. <https://doi.org/10.1029/2020WR029500>
- 884 Craig, H., Gordon, L. I., & Horibe, Y. (1964). Isotopic exchange effects in the evaporation of water: 1.
885 Low-temperature experimental results. *Journal of Geophysical Research*, 68(17), 5079–5087.
886 <https://doi.org/10.1029/JZ068I017P05079>
- 887 Dawson, T., & Ehleringer, J. (1991). Streamside trees that do not use stream water. *Nature*, 350, 335–
888 337. <https://doi.org/10.1038/350335a0>
- 889 Dick, J. J., Tetzlaff, D., Birkel, C., & Soulsby, C. (2015). Modelling landscape controls on dissolved
890 organic carbon sources and fluxes to streams. *Biogeochemistry*, 122(2–3), 361–374.
891 <https://doi.org/10.1007/S10533-014-0046-3>
- 892 Donnelly, C., Andersson, J. C. M., & Arheimer, B. (2016). Using flow signatures and catchment
893 similarities to evaluate the E-HYPE multi-basin model across Europe. *Hydrological Sciences*
894 *Journal*, 61(2), 255–273. <https://doi.org/10.1080/02626667.2015.1027710>

895 Eckersten, H., Jansson, P. E., & Johnsson, H. (1994). SOILN model – user’s manual 2nd edition, Division
896 of Agricultural Hydrotechnics Communications, 94:4. Department of Soil Sciences, Swedish
897 University of Agricultural Sciences, 58pp, Uppsala.

898 Efstratiadis, A., & Koutsoyiannis, D. (2010). One decade of multi-objective calibration approaches in
899 hydrological modelling: A review. *Hydrological Sciences Journal*, 55(1), 58–78.
900 <https://doi.org/10.1080/02626660903526292>

901 Godsey, S. E., Aas, W., Clair, T. A., de Wit, H. A., Fernandez, I. J., Kahl, J. S., et al. (2010). Generality of
902 fractal 1/f scaling in catchment tracer time series, and its implications for catchment travel
903 time distributions. *Hydrological Processes*, 24(12), 1660–1671.
904 <https://doi.org/10.1002/hyp.7677>

905 Good, S. P., Soderberg, K., Guan, K., King, E. G., Scanlon, T. M., & Caylor, K. K. (2014). $\delta^2\text{H}$ isotopic flux
906 partitioning of evapotranspiration over a grass field following a water pulse and subsequent
907 dry down. *Water Resources Research*, 50(2), 1410–1432.
908 <https://doi.org/10.1002/2013WR014333>

909 Grizzetti, B., Vigiak, O., Udias, A., Aloe, A., Zanni, M., Bouraoui, F., et al. (2021). How EU policies could
910 reduce nutrient pollution in European inland and coastal waters. *Global Environmental*
911 *Change*, 69, 102281. <https://doi.org/10.1016/j.gloenvcha.2021.102281>

912 Hersbach, H., Bell, B., Berrisford, P., Hirahara, S., Horányi, A., Muñoz Sabater, J., et al. (2020). The ERA5
913 global reanalysis. *Quarterly Journal of the Royal Meteorological Society*, 146.
914 <https://doi.org/10.1002/qj.3803>

915 Hooper, R., Stone, A., Christophersen, N., de Melo, E., & Seip, H. (1988). Assessing the Birkenes Model
916 of Stream Acidification using a multi-signal calibration methodology. *Water Resources*
917 *Research - WATER RESOUR RES*, 24, 1308–1316. <https://doi.org/10.1029/WR024i008p01308>

918 Horita, J., Rozanski, K., & Cohen, S. (2008). Isotope effects in the evaporation of water: A status report
919 of the Craig-Gordon model. *Isotopes in Environmental and Health Studies*, 44, 23–49.
920 <https://doi.org/10.1080/10256010801887174>

921 Hrachowitz, M., Savenije, H., Bogaard, T. A., Tetzlaff, D., & Soulsby, C. (2013). What can flux tracking
922 teach us about water age distribution patterns and their temporal dynamics? *Hydrology and*
923 *Earth System Sciences*, 17(2), 533–564. <https://doi.org/10.5194/HESS-17-533-2013>

924 Huijgevoort, M., Tetzlaff, D., & Sutanudjaja, E. (2016). Using high resolution tracer data to constrain
925 water storage, flux and age estimates in a spatially distributed rainfall-runoff model.
926 *Hydrological Processes*, 30. <https://doi.org/10.1002/hyp.10902>

927 Jasechko, S., Kirchner, J., Welker, J., & McDonnell, J. (2016). Substantial proportion of global
928 streamflow less than three months old. *Nature Geoscience*, 9.
929 <https://doi.org/10.1038/NCEO2636>

930 Jones, E. R., Bierkens, M. F. P., Wanders, N., Sutanudjaja, E. H., van Beek, L. P. H., & van Vliet, M. T. H.
931 (2023). DynQual v1.0: a high-resolution global surface water quality model. *Geoscientific*
932 *Model Development*, 16(15), 4481–4500. <https://doi.org/10.5194/gmd-16-4481-2023>

933 Jung, H., Tetzlaff, D., Birkel, C., & Soulsby, C. (2025). Recent Developments and Emerging Challenges
934 in Tracer-Aided Modeling. *Wiley Interdisciplinary Reviews Water*, 12.
935 <https://doi.org/10.1002/wat2.70015>

936 Kale, R., & Sahoo, B. (2011). Green-Ampt Infiltration Models for Varied Field Conditions: A Revisit.
937 *Water Resources Management*, 25, 3505–3536. <https://doi.org/10.1007/s11269-011-9868-0>

938 Kumar, R., Samaniego, L., & Attinger, S. (2013). Implications of distributed hydrologic model
939 parameterization on water fluxes at multiple scales and locations. *Water Resources Research*,
940 49(1), 360–379. <https://doi.org/10.1029/2012WR012195>

- 941 Kuppel, S., Tetzlaff, D., Maneta, M., & Soulsby, C. (2018). EcH2O-iso 1.0: Water isotopes and age
 942 tracking in a process-based, distributed ecohydrological model. *Geoscientific Model*
 943 *Development*, 11, 3045–3069. <https://doi.org/10.5194/gmd-11-3045-2018>
- 944 Landgraf, J., Tetzlaff, D., Birkel, C., Stevenson, J., & Soulsby, C. (2023). Assessing land use effects on
 945 ecohydrological partitioning in the critical zone through isotope-aided modelling. *Earth*
 946 *Surface Processes and Landforms*, 48. <https://doi.org/10.1002/esp.5691>
- 947 Lindström, G., Pers, C., Rosberg, J., Strömqvist, J., & Arheimer, B. (2010). Development and test of the
 948 HYPE (Hydrological Predictions for the Environment) model – A water quality model for
 949 different spatial scales. *Hydrology Research*, 41. <https://doi.org/10.2166/nh.2010.007>
- 950 Maneta, M. P., & Silverman, N. L. (2013). A spatially distributed model to simulate water, energy, and
 951 vegetation dynamics using information from regional climate models. *Earth Interactions*,
 952 17(11), 1–44. <https://doi.org/10.1175/2012EI000472.1>
- 953 McDonnell, J. (2014). The two water worlds hypothesis: Ecohydrological separation of water between
 954 streams and trees? *Wiley Interdisciplinary Reviews: Water*, 1.
 955 <https://doi.org/10.1002/wat2.1027>
- 956 McDonnell, J., & Beven, K. (2014). Debates on Water Resources: The future of hydrological sciences:
 957 A (common) path forward? A call to action aimed at understanding velocities, celerities and
 958 residence time distributions of the headwater hydrograph. *Water Resources Research*, 50.
 959 <https://doi.org/10.1002/2013WR015141>
- 960 Mcmillan, H., Araki, R., Bolotin, L., Kim, D.-H., Coxon, G., Clark, M., & Seibert, J. (2025). Global patterns
 961 in observed hydrologic processes. *Nature Water*, 3. <https://doi.org/10.1038/s44221-025-00407-w>
- 962
- 963 Mikayilov, F., Rouholahnejad Freund, E., Ashraf Vaghefi, S., Srinivasan, R., Yang, H., & Klöve, B. (2015).
 964 A continental-scale hydrology and water quality model for Europe: Calibration and uncertainty
 965 of a high-resolution large-scale SWAT model. *Journal of Hydrology*, 524.
 966 <https://doi.org/10.1016/j.jhydrol.2015.03.027>
- 967 Mu, Q., Zhao, M., & Running, S. (2011). Improvements to a MODIS Global Terrestrial
 968 Evapotranspiration Algorithm. *Remote Sensing of Environment*, 115, 1781–1800.
 969 <https://doi.org/10.1016/j.rse.2011.02.019>
- 970 Nan, Y., He, Z., Tian, F., Wei, Z., & Tian, L. (2021). Can we use precipitation isotope outputs of isotopic
 971 general circulation models to improve hydrological modeling in large mountainous
 972 catchments on the Tibetan Plateau? *Hydrology and Earth System Sciences*, 25(12), 6151–6172.
 973 <https://doi.org/10.5194/hess-25-6151-2021>
- 974 Naz, B. S., Sharples, W., Ma, Y., Goergen, K., & Kollet, S. (2023). Continental-scale evaluation of a fully
 975 distributed coupled land surface and groundwater model, ParFlow-CLM (v3.6.0), over Europe.
 976 *Geoscientific Model Development*, 16(6), 1617–1639. <https://doi.org/10.5194/gmd-16-1617-2023>
- 977
- 978 Neal, C., Christophersen, N., Neale, R., Smith, C., & Reynolds, B. (1988). Chloride in precipitation and
 979 streamwater for the upland catchment of River Severn, mid- Wales; some consequences for
 980 hydrochemical models. *Hydrological Processes*, 2, 155–165.
 981 <https://doi.org/10.1002/hyp.3360020206>
- 982 Nearing, G., Ruddell, B., Bennett, A., Prieto, C., & Gupta, H. (2020). Does Information Theory Provide
 983 a New Paradigm for Earth Science? Hypothesis Testing. *Water Resources Research*, 56.
 984 <https://doi.org/10.1029/2019WR024918>
- 985 Ocampo, C., Sivapalan, M., & Oldham, C. (2006). Hydrological connectivity of upland-riparian zones in
 986 agricultural catchments: Implications for runoff generation and nitrate transport. *Journal of*
 987 *Hydrology*, 331, 643–658. <https://doi.org/10.1016/j.jhydrol.2006.06.010>

- 988 Pechlivanidis, I., Jackson, B., Mcintyre, N., & Wheeler, H. (2011). Catchment scale hydrological
989 modelling: A review of model types, calibration approaches and uncertainty analysis methods
990 in the context of recent developments in technology and applications. *GlobalNEST*
991 *International Journal*, 13, 193–214.
- 992 Pesántez, J., Birkel, C., Gaona, G., Arciniega-Esparza, S., Murray, D., Mosquera, G., et al. (2023).
993 Spatially distributed tracer-aided modelling to explore DOC dynamics, hot spots and hot
994 moments in a tropical mountain catchment. *Hydrological Processes*, 37, 1–15.
995 <https://doi.org/10.1002/hyp.15020>
- 996 Rakovec, O., Kumar, R., Mai, J., Cuntz, M., Thober, S., Zink, M., et al. (2016). Multiscale and Multivariate
997 Evaluation of Water Fluxes and States over European River Basins. *Journal of*
998 *Hydrometeorology*, 17, 287–307. <https://doi.org/10.1175/JHM-D-15-0054.1>
- 999 Rakovec, O., Mizukami, N., Kumar, R., Newman, A., Thober, S., Wood, A., et al. (2019). Diagnostic
1000 Evaluation of Large-Domain Hydrologic Models Calibrated Across the Contiguous United
1001 States. *Journal of Geophysical Research: Atmospheres*, 124.
1002 <https://doi.org/10.1029/2019JD030767>
- 1003 Remondi, F., Kirchner, J., Burlando, P., & Fatichi, S. (2018). Water Flux Tracking with A Distributed
1004 Hydrological Model to Quantify Controls on the Spatio-Temporal Variability of Transit Time
1005 Distributions. *Water Resources Research*, 54. <https://doi.org/10.1002/2017WR021689>
- 1006 Samaniego, L., Kumar, R., & Attinger, S. (2010). Multiscale parameter regionalization of a grid-based
1007 hydrologic model at the mesoscale. *Water Resour. Res.*, 46.
1008 <https://doi.org/10.1029/2008WR007327>
- 1009 Seybold, E., Dwivedi, R., Musselman, K., Kincaid, D., Schroth, A., Classen, A., et al. (2022). Winter runoff
1010 events pose an unquantified continental-scale risk of high wintertime nutrient export.
1011 *Environmental Research Letters*, 17, 104044. <https://doi.org/10.1088/1748-9326/ac8be5>
- 1012 Šimůnek, J., Šejna, M., Saito, H., & Van Genuchten, M. T. (2013). *The HYDRUS-1D software package*
1013 *for simulating the one-dimensional movement of water, heat, and multiple solutes in variably-*
1014 *saturated media (Version 4.17)*. Department of Environmental Sciences University of Riverside
1015 California, California.
- 1016 Skrzypek, G., Mydłowski, A., Dogramaci, S., Hedley, P., Gibson, J. J., & Grierson, P. F. (2015). Estimation
1017 of evaporative loss based on the stable isotope composition of water using Hydrocalculator.
1018 *Journal of Hydrology*, 523, 781–789. <https://doi.org/10.1016/J.JHYDROL.2015.02.010>
- 1019 Smith, A., Tetzlaff, D., Kleine, L., Maneta, M., & Soulsby, C. (2021). Quantifying the effects of land use
1020 and model scale on water partitioning and water ages using tracer-aided ecohydrological
1021 models. *Hydrology and Earth System Sciences*, 25, 2239–2259. [https://doi.org/10.5194/hess-](https://doi.org/10.5194/hess-25-2239-2021)
1022 [25-2239-2021](https://doi.org/10.5194/hess-25-2239-2021)
- 1023 Soulsby, C., Birkel, C., Geris, J., Dick, J., Tunaley, C., & Tetzlaff, D. (2015). Stream water age distributions
1024 controlled by storage dynamics and nonlinear hydrologic connectivity: Modeling with high-
1025 resolution isotope data. *Water Resources Research*, 51(9), 7759–7776.
1026 <https://doi.org/10.1002/2015WR017888>
- 1027 Sprenger, M., Stumpp, C., Weiler, M., Aeschbach, W., Allen, S., Benettin, P., et al. (2019). The
1028 Demographics of Water: A Review of Water Ages in the Critical Zone. *Reviews of Geophysics*,
1029 57. <https://doi.org/10.1029/2018RG000633>
- 1030 Tapley, B., Bettadpur, S., Ries, J. C., Thompson, P., & Watkins, M. (2004). GRACE Measurements of
1031 Mass Variability in the Earth System. *Science (New York, N.Y.)*, 305, 503–5.
1032 <https://doi.org/10.1126/science.1099192>
- 1033 Tetzlaff, D., Buttle, J., Carey, S. K., Mcguire, K., Laudon, H., & Soulsby, C. (2015). Tracer-based
1034 assessment of flow paths, storage and runoff generation in northern catchments: A review.
1035 *Hydrological Processes*, 29(16), 3475–3490. <https://doi.org/10.1002/HYP.10412>

- 1036 Wang, J., Bouwman, A., Vilmin, L., Beusen, A., Hoek, W., Liu, X., & Middelburg, J. (2024). Global inland-
 1037 water nitrogen cycling has accelerated in the Anthropocene. *Nature Water*, 2.
 1038 <https://doi.org/10.1038/s44221-024-00282-x>
- 1039 Wellen, C., Kamran-Disfani, A.-R., & Arhonditsis, G. (2015). Evaluation of the Current State of
 1040 Distributed Watershed Nutrient Water Quality Modeling. *Environmental Science &*
 1041 *Technology*, 49. <https://doi.org/10.1021/es5049557>
- 1042 Wen, Y., Lin, J.-S., Plaza, F., & Liang, X. (2024). Roles of Hydrology and Transport Processes in
 1043 Denitrification at Watershed Scale. *Water Resources Research*, 60, 1–24.
 1044 <https://doi.org/10.1029/2023WR034971>
- 1045 Winkler, K., Fuchs, R., Rounsevell, M., & Herold, M. (2021). Global land use changes are four times
 1046 greater than previously estimated. *Nature Communications*, 12(1), 2501.
 1047 <https://doi.org/10.1038/s41467-021-22702-2>
- 1048 Wu, S., Tetzlaff, D., Yang, X., & Soulsby, C. (2022). Disentangling the influence of landscape
 1049 characteristics, hydroclimatic variability and land management on surface water NO₃-N
 1050 dynamics: spatially distributed modelling over 30 years in a lowland mixed land use catchment.
 1051 *Water Resources Research*, e2021WR030566. <https://doi.org/10.1029/2021WR030566>
- 1052 Wu, S., Tetzlaff, D., Beven, K., & Soulsby, C. (2025a). DREAM(LoAX): Simultaneous Calibration and
 1053 Diagnosis for Tracer-Aided Ecohydrological Models Under the Equifinality Thesis. *Water*
 1054 *Resources Research*, 61, e2024WR038779. <https://doi.org/10.1029/2024WR038779>
- 1055 Wu, S., Tetzlaff, D., Yang, X., Sauter, T., & Soulsby, C. (2025b). Hydrological Connectivity Dominates
 1056 NO₃-N Cycling in Complex Landscapes – Insights From Integration of Isotopes and Water
 1057 Quality Modeling. *Water Resources Research*, 61, e2025WR040525.
 1058 <https://doi.org/10.1029/2025WR040525>
- 1059 Wu, S., Tetzlaff, D., & Soulsby, C. (2025c). Revising Common Approaches for Calibration: Insights From
 1060 a 1-D Tracer-Aided Hydrological Model With High-Dimensional Parameters and Objectives.
 1061 *Water Resources Research*, 61, e2024WR037656. <https://doi.org/10.1029/2024WR037656>
- 1062 Wu, S., Tetzlaff, D., Zheng, Y., & Soulsby, C. (2025d). EcoTWIN v1.0 release.
 1063 <https://doi.org/10.5281/zenodo.16747633>
- 1064 Yang, C., Condon, L., & Maxwell, R. (2025). Unravelling groundwater–stream connections over the
 1065 continental United States. *Nature Water*, 3. <https://doi.org/10.1038/s44221-024-00366-8>
- 1066 Yang, X., Jomaa, S., Zink, M., Fleckenstein, J., Borchardt, D., & Rode, M. (2018). A New Fully Distributed
 1067 Model of Nitrate Transport and Removal at Catchment Scale. *Water Resources Research*, 54.
 1068 <https://doi.org/10.1029/2017WR022380>
- 1069 Yang, X., Zhang, X., Graeber, D., Hensley, R., Jarvie, H., Lorke, A., et al. (2023a). Large-stream nitrate
 1070 retention patterns shift during droughts: Seasonal to sub-daily insights from high-frequency
 1071 data-model fusion. *Water Research*, 243, 120347.
 1072 <https://doi.org/10.1016/j.watres.2023.120347>
- 1073 Yang, X., Tetzlaff, D., Müller, C., Knöller, K., Borchardt, D., & Soulsby, C. (2023b). Upscaling Tracer-
 1074 Aided Ecohydrological Modeling to Larger Catchments: Implications for Process
 1075 Representation and Heterogeneity in Landscape Organization. *Water Resources Research*, 59,
 1076 e2022WR033033. <https://doi.org/10.1029/2022WR033033>
- 1077 Yang, X., Tetzlaff, D., Jin, J., Li, Q., Borchardt, D., & Soulsby, C. (2024). Linking terrestrial biogeochemical
 1078 processes and water ages to catchment water quality: A new Damköhler analysis based on
 1079 coupled modeling of isotope tracers and nitrate dynamics. *Water Research*, 262, 122118.
 1080 <https://doi.org/10.1016/j.watres.2024.122118>
- 1081 Zhang, Z., Chen, X., Cheng, Q.-B., Li, S.-L., Yue, F.-J., Peng, T., et al. (2020). Coupled hydrological and
 1082 biogeochemical modelling of nitrogen transport in the karst critical zone. *Science of The Total*
 1083 *Environment*, 732, 138902. <https://doi.org/10.1016/j.scitotenv.2020.138902>

1084 Zhu, J., Jia, Y., Yu, G., Wang, Q., He, N., Chen, Z., et al. (2025). Changing patterns of global nitrogen
1085 deposition driven by socio-economic development. *Nature Communications*, 16(1), 46.
1086 <https://doi.org/10.1038/s41467-024-55606-y>
1087